Space-Time Correlated Mobile-to-Mobile Channels: Modelling and Simulation

Alenka G. Zajić, *Student Member, IEEE*, and Gordon L. Stüber, *Fellow, IEEE*

***Abstract*—A *single- and double-bounced two-ring* parametric reference model is proposed for multiple-input multiple-output (MIMO) mobile-to-mobile (M-to-M) Ricean fading channels. From this model, a closed-form joint space-time correlation function and a space-Doppler power spectrum are derived for a two-dimensional (2-D) non-isotropic scattering environment. Also, space-time correlation functions for the in-phase and quadrature components of the complex faded envelope are derived, assuming a 2-D isotropic scattering environment. Finally, two new sum-of-sinusoids based simulation models for MIMO M-to-M Ricean fading channels are proposed. The statistics of the simulation models are verified by simulation. The results show that the simulation models are a good approximation of the reference model and that they outperform existing simulation models.**

***Index Terms*—Deterministic and statistical methods, Doppler spectrum, fading channel simulator, mobile-to-mobile channels, Ricean and Rayleigh fading, sum-of-sinusoids.**

I. Introduction

MOBILE *ad-hoc* wireless networks, intelligent transportation systems, and relay-based cellular networks all use mobile-to-mobile (M-to-M) communication channels, where both the transmitter $(\mathrm{T_x})$ and the receiver $(\mathrm{R_x})$ are in motion and equipped with low elevation antennas. M-to-M channels differ from conventional fixed-to-mobile (F-to-M) cellular radio channels, where the base-station is stationary, elevated, and relatively free of local scattering. Akki and Haber [1], [2] showed that the received envelope on M-to-M channels is Rayleigh faded under non line-of-sight conditions (NLoS), but the statistical properties differ from F-to-M channels. They were the first to propose a reference model for single-input single-output (SISO) M-to-M Rayleigh fading channels. Methods for simulating SISO M-to-M channels have been proposed in [3]–[5]. Channel measurements for narrowband and wideband mobile-to-mobile communications have been reported in [6] and [7], respectively. Recently, using the "two-ring" geometrical model in [8], Pätzold *et al.* proposed a reference model for narrowband MIMO M-to-M channel [9]. Based on this reference model, they also proposed a deterministic sum-of-sinusoids (SoS) model called the Modified Method of Exact Doppler Spreads (MMEDS) [10].

Previously reported models for MIMO M-to-M channels [9], [10] consider radio propagation in outdoor macro-cells, assuming that all rays are only double-bounced. This paper first proposes a new parametric reference model that employs a two-ring model and constructs the received complex faded envelope as a superposition of the line-of-sight (LoS), single-bounced, and double-bounced rays. The parametric nature of the model makes it adaptable to a variety of propagation environments, i.e., outdoor micro—and macro-cells. For example, our reference model describes the radio propagation in outdoor macro-cells as a combination of single- and double-bounced rays, taking into account that the double-bounced rays bear more energy than the single-bounced rays. In particular, if there are no single-bounced and LoS rays, our model simplifies to the model proposed in [9] and [10]. From the new reference model, we derive a closed-form joint space-time correlation function for a two-dimensional (2-D) non-isotropic scattering environment. For 2-D isotropic scattering and no single-bounced and LoS rays, our space-time correlation function is shown to reduce to the one derived in [9]. Furthermore, we derive the space-time correlation functions of the in-phase (I) and quadrature (Q) components of the complex faded envelope for the 2-D isotropic scattering environment. Finally, we derive the space-Doppler power spectrum of the complex faded envelope assuming a 2-D non-isotropic scattering environment.

The reference models assume an infinite number of scatterers, which prevents practical implementation. Hence, we propose an ergodic statistical (deterministic) SoS simulation model for a 2-D isotropic scattering environment. We employ a "two-ring" model that combines the LoS, single-bounced, and double-bounced rays and has orthogonal functions as the I and Q components of the complex faded envelope. The statistical properties of our model are verified by simulations. Furthermore, by allowing amplitudes, phases, and Doppler frequencies to be random variables, the deterministic model is modified to better match statistical properties of the reference model. This model is called the statistical simulation model. The statistical properties of the statistical model vary for each simulation trial, but will converge to desired ensemble averaged properties when averaged over a sufficient number of simulation trials. The statistical properties of this model are also verified by simulations. Finally, we compare the performance and complexity of our new models with the MMEDS model. For fair comparison, we remove the LoS and single-bounced components of the complex faded envelope from our models. Our deterministic model performs similar to the MMEDS model [10], but requires

Manuscript received May 30, 2006; revised December 15, 2006, April 8, 2006, and June 4, 2007. The review of this paper was coordinated by Prof. Y. Ma. This work was prepared through collaborative participation in the Collaborative Technology Alliance for Communications and Networks sponsored by the U.S. Army Research Laboratory under Cooperative Agreement DAAD19-01-2-0011. The U.S. Government is authorized to reproduce and distribute reprints for Government purposes notwithstanding any copyright notation thereon. The views and conclusions contained in this document are those of the authors and should not be interpreted as representing the official policies, either expressed or implied, of the Army Research Laboratory or the U.S. Government.

The authors are with the School of Electrical and Computer Engineering, Georgia Institute of Technology, Atlanta, GA 30332 USA (e-mail: alenka@ece.gatech.edu; stuber@ece.gatech.edu).

Digital Object Identifier 10.1109/TVT.2007.905591

a smaller number of scatterers and has a shorter simulation time. Compared to the deterministic and the MMEDS model, the statistical properties of the statistical model match those of the reference model over a wider range of normalized time delays while using smaller number of scatterers.

The remainder of the paper is organized as follows. Section II describes the communication system and presents the new parametric reference model for MIMO M-to-M channels. Section III presents the derivation of the closed-form joint space-time correlation function for 2-D non-isotropic scattering, the derivation of the space-time correlation functions of the I and Q components of the complex faded envelope for 2-D isotropic scattering, and the derivation of the space-Doppler power spectrum of the complex faded envelope for 2-D non-isotropic scattering. Section IV reviews the MMEDS model proposed in [10] and details the deterministic and statistical simulation models. Section V presents simulation results for our new models and compares them to the MMEDS model in [10]. Section VI provides some concluding remarks.

II. A New Parametric Reference Model for MIMO Mobile-to-Mobile Channels

This paper considers a narrowband single-user MIMO communication system with L_t transmit and L_r receive omnidirectional antenna elements. It is assumed that both the $\mathrm{T_x}$ and $\mathrm{R_x}$ are in motion and equipped with low elevation antennas. This paper considers the radio propagation in outdoor micro- and macro-cells, which is characterized by 2-D scattering with either line-of-sight (LoS) or non-line-of-sight (NLoS) conditions between the transmitter and receiver. The MIMO channel can be described by an $L_r \times L_t$ matrix $\mathbf{H}(t) = [h_{ij}(t)]_{L_r \times L_t}$ of complex faded envelopes.

The geometry of the proposed model is shown in Figs. 1 and 2. Fig. 1 shows the two-ring model with single- and double-bounced rays for a MIMO M-to-M channel with $L_t = L_r = 2$ antenna elements. Fig. 2 shows the LoS paths for the channel in Fig. 1. This elementary 2×2 antenna configuration will be used later to construct uniform linear antenna arrays with arbitrary number of antennas. The two-ring model defines two rings of fixed scatterers, one around the $\mathrm{T_x}$ and another around the $\mathrm{R_x}$, as shown in Fig. 1. Around the transmitter, M omnidirectional scatterers lie on a ring of radius R_t, and the mth transmit scatterer is denoted by $S_T^{(m)}$. Similarly, around the receiver, N omnidirectional scatterers lie on a ring of radius R_r and the nth receive scatterer is denoted by $S_R^{(n)}$. The distance between the $\mathrm{T_x}$ and $\mathrm{R_x}$ is D. It is assumed that the radii R_t and R_r are much smaller than the distance D between the $\mathrm{T_x}$ and $\mathrm{R_x}$, i.e., $\max\{R_t, R_r\} \ll D$ (local scattering condition). Furthermore, it is assumed that the distance D is smaller than $4R_tR_rL_r/(\lambda(L_t-1)(L_r-1))$ (channel does not experience keyhole behavior [11]), where λ denotes the carrier wavelength. The spacing between two adjacent antenna elements at the $\mathrm{T_x}$ and $\mathrm{R_x}$ is denoted by δ_T and δ_R, respectively. It is assumed that δ_T and δ_R are much smaller than the radii R_t and R_r, i.e., $\max\{\delta_T, \delta_R\} \ll \min\{R_t, R_r\}$. Angles θ_T and θ_R describe the orientation of the $\mathrm{T_x}$ and $\mathrm{R_x}$ antenna array, respectively, relative to the x-axis. Similarly, the $\mathrm{T_x}$ and $\mathrm{R_x}$ are moving with speeds v_T and v_R in directions described by angles γ_T and γ_R, respectively. In Fig. 1, the symbols $\alpha_T^{(m)}$ and $\alpha_T^{(n)}$ are

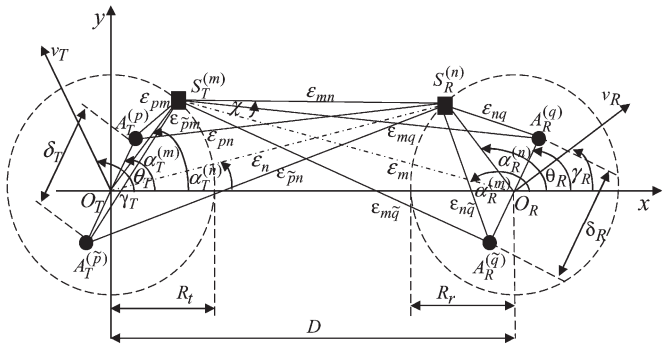

Fig. 1. Single- and double-bounced two-ring model for MIMO M-to-M channel with $L_t = L_r = 2$ antenna elements.

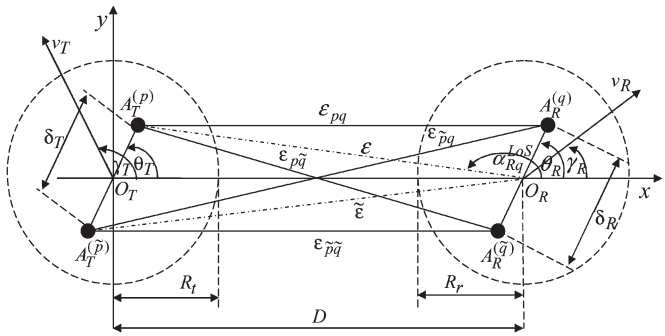

Fig. 2. LoS paths in the 2×2 channel of Fig. 1.

the angles of departure (AoD) of the waves that impinge on the scatterers $S_T^{(m)}$ and $S_R^{(n)}$, whereas $\alpha_R^{(m)}$ and $\alpha_R^{(n)}$ are the angles of arrival (AoA) of the waves scattered from $S_T^{(m)}$ and $S_R^{(n)}$, respectively. The symbols ϵ_{pm}, ϵ_{mq}, ϵ_{pn}, ϵ_{nq}, and ϵ_{mn} denote distances $A_T^{(p)} - S_T^{(m)}$, $S_T^{(m)} - A_R^{(q)}$, $A_T^{(p)} - S_R^{(n)}$, $S_R^{(n)} - A_R^{(q)}$, and $S_T^{(m)} - S_R^{(n)}$, respectively, as shown in Fig. 1. In Fig. 2, the symbols α_{Rq}^{LoS} and ϵ_{pq} denote the AoAs of the LoS paths and the distance $A_T^{(p)} - A_R^{(q)}$, respectively.

From the geometrical model described above, the received complex faded envelope of the link $A_T^{(p)} - A_R^{(q)}$ is a superposition of the LoS, the single-bounced, and the double-bounced rays, and can be written as follows:

$$h_{pq}(t) = h_{pq}^{SBT}(t) + h_{pq}^{SBR}(t) + h_{pq}^{DB}(t) + h_{pq}^{LoS}(t) \qquad (1)$$

where the single-bounced components of the received complex faded envelope are, respectively

$$h_{pq}^{SBT}(t) = \sqrt{\frac{\eta_T \Omega_{pq}}{K_{pq}+1}} \lim_{M\to\infty} \sum_{m=1}^{M} \frac{1}{\sqrt{M}} e^{j\phi_m - j\frac{2\pi}{\lambda}(\epsilon_{pm}+\epsilon_{mq})} \times e^{j2\pi t\left[f_{T\max}\cos\left(\alpha_T^{(m)}-\gamma_T\right)+f_{R\max}\cos\left(\alpha_R^{(m)}-\gamma_R\right)\right]} \qquad (2)$$

$$h_{pq}^{SBR}(t) = \sqrt{\frac{\eta_R \Omega_{pq}}{K_{pq}+1}} \lim_{N\to\infty} \sum_{n=1}^{N} \frac{1}{\sqrt{N}} e^{j\phi_n - j\frac{2\pi}{\lambda}(\epsilon_{pn}+\epsilon_{nq})} \times e^{j2\pi t\left[f_{T\max}\cos\left(\alpha_T^{(n)}-\gamma_T\right)+f_{R\max}\cos\left(\alpha_R^{(n)}-\gamma_R\right)\right]} \qquad (3)$$

the double-bounced component of the received complex faded envelope is

$$h_{pq}^{DB}(t)=\sqrt{\frac{\eta_{TR}\Omega_{pq}}{K_{pq}+1}}\lim_{M,N\to\infty}\sum_{m,n=1}^{M,N}\frac{1}{\sqrt{MN}}e^{-j\frac{2\pi}{\lambda}(\epsilon_{pm}+\epsilon_{mn}+\epsilon_{nq})}\times e^{j2\pi t\left[f_{T\max}\cos\left(\alpha_T^{(m)}-\gamma_T\right)+f_{R\max}\cos\left(\alpha_R^{(n)}-\gamma_R\right)\right]+j\phi_{mn}} \quad (4)$$

and the LoS component of the received complex faded envelope is

$$h_{pq}^{LoS}(t)=\sqrt{\frac{K_{pq}\Omega_{pq}}{K_{pq}+1}}e^{j2\pi t f_{T\max}\cos\left(\pi-\alpha_{Rq}^{LoS}-\gamma_T\right)}\times e^{j2\pi t f_{R\max}\cos\left(\alpha_{Rq}^{LoS}-\gamma_R\right)-j\frac{2\pi}{\lambda}\epsilon_{pq}}. \quad (5)$$

In (2)–(5), Ω_{pq} and K_{pq} denote the transmitted power and the Ricean factor of the subchannel $A_T^{(p)}-A_R^{(q)}$, respectively. Parameters η_T, η_R, and η_{TR} specify how much the single- and double-bounced rays contribute in the total power Ω_{pq}, i.e., these parameters satisfy $\eta_T+\eta_R+\eta_{TR}=1$. Frequencies $f_{T\max}=v_T/\lambda$ and $f_{R\max}=v_R/\lambda$ are the maximum Doppler frequencies associated with the $\mathrm{T_x}$ and $\mathrm{R_x}$, respectively, and λ is the carrier wavelength. It is assumed that the AoDs ($\alpha_T^{(m)}$ and $\alpha_T^{(n)}$) and the AoAs ($\alpha_R^{(m)}$ and $\alpha_R^{(n)}$) are random variables. Note that double-bounced rays have the AoD, $\alpha_T^{(m)}$, independent from the AoA, $\alpha_R^{(n)}$, [11], whereas single-bounced rays have the AoA, $\alpha_R^{(m)}$, dependent on the AoD, $\alpha_T^{(m)}$, and the AoD, $\alpha_T^{(n)}$, dependent on the AoA $\alpha_R^{(n)}$ (see Appendix). Finally, it is assumed that the phases ϕ_m, ϕ_n, and ϕ_{mn} are random variables uniformly distributed on the interval $[-\pi,\pi)$ and independent from the angles of departure and the angles of arrival.

As shown in the Appendix, the distances ϵ_{pm}, ϵ_{mq}, ϵ_{pn}, ϵ_{nq}, ϵ_{mn}, and ϵ_{pq} can be expressed as functions of the angles $\alpha_T^{(m)}$, $\alpha_R^{(n)}$, and α_{Rq}^{LoS} as follows:

$$\epsilon_{pm}\approx R_t-(0.5L_t+0.5-p)\delta_T\cos\left(\theta_T-\alpha_T^{(m)}\right) \quad (6)$$

$$\epsilon_{mq}\approx D-(0.5L_r+0.5-q)\times\delta_R\left[\Delta_T\sin\theta_R\sin\alpha_T^{(m)}-\cos\theta_R\right] \quad (7)$$

$$\epsilon_{pn}\approx D-(0.5L_t+0.5-p)\times\delta_T\left[\Delta_R\sin\theta_T\sin\alpha_R^{(n)}+\cos\theta_T\right] \quad (8)$$

$$\epsilon_{nq}\approx R_r-(0.5L_r+0.5-q)\delta_R\cos\left(\alpha_R^{(n)}-\theta_R\right) \quad (9)$$

$$\epsilon_{mn}=\epsilon_m\frac{\sin\left(\alpha_R^{(m)}-\alpha_R^{(n)}\right)}{\sin\left(\chi+\left(\alpha_R^{(m)}-\alpha_R^{(n)}\right)\right)}\approx D \quad (10)$$

$$\epsilon_{pq}\approx D-(0.5L_t+0.5-p)\delta_T\cos\theta_T-(0.5L_r+0.5-q)\delta_R\cos\left(\alpha_{Rq}^{LoS}-\theta_R\right) \quad (11)$$

where parameters p and q take values from the sets $p\in\{1,\ldots,L_t\}$ and $q\in\{1,\ldots,L_r\}$, respectively, $\Delta_T=R_t/D$, and $\Delta_R=R_r/D$.

Using (6)–(11), the single-bounced, double-bounced, and LoS components of the complex faded envelope become, respectively

$$h_{pq}^{SBT}(t)=\sqrt{\frac{\eta_T\Omega_{pq}}{K_{pq}+1}}\lim_{M\to\infty}\sum_{m=1}^{M}\frac{e^{j\frac{\pi}{\lambda}(L_t+1-2p)\delta_T\cos\left(\theta_T-\alpha_T^{(m)}\right)}}{\sqrt{M}}\times e^{j\phi_m-j\frac{2\pi}{\lambda}(D+R_t)+j\frac{\pi}{\lambda}(L_r+1-2q)\delta_R\left[\Delta_T\sin\theta_R\sin\alpha_T^{(m)}-\cos\theta_R\right]}\times e^{j2\pi t\left[f_{T\max}\cos\left(\alpha_T^{(m)}-\gamma_T\right)+f_{R\max}\left(\Delta_T\sin\gamma_R\sin\alpha_T^{(m)}-\cos\gamma_R\right)\right]} \quad (12)$$

$$h_{pq}^{SBR}(t)=\sqrt{\frac{\eta_R\Omega_{pq}}{K_{pq}+1}}\lim_{N\to\infty}\times\sum_{n=1}^{N}\frac{e^{j\frac{\pi}{\lambda}(L_r+1-2q)\delta_R\cos\left(\alpha_R^{(n)}-\theta_R\right)}}{\sqrt{N}}\times e^{j\phi_n-j\frac{2\pi}{\lambda}(D+R_r)+j\frac{\pi}{\lambda}(L_t+1-2p)\delta_T\left[\Delta_R\sin\theta_T\sin\alpha_R^{(n)}+\cos\theta_T\right]}\times e^{j2\pi t\left[f_{R\max}\cos\left(\alpha_R^{(n)}-\gamma_R\right)+f_{T\max}\left(\Delta_R\sin\gamma_T\sin\alpha_R^{(n)}+\cos\gamma_T\right)\right]} \quad (13)$$

$$h_{pq}^{DB}(t)=\sqrt{\frac{\eta_{TR}\Omega_{pq}}{K_{pq}+1}}\lim_{M,N\to\infty}\sum_{m,n=1}^{M,N}\frac{e^{-j\frac{2\pi}{\lambda}(D+R_t+R_r)+j\phi_{mn}}}{\sqrt{MN}}\times e^{j\frac{\pi}{\lambda}(L_t+1-2p)\delta_T\cos\left(\theta_T-\alpha_T^{(m)}\right)+j\frac{\pi}{\lambda}(L_r+1-2q)\delta_R\cos\left(\alpha_R^{(n)}-\theta_R\right)}\times e^{j2\pi t\left[f_{T\max}\cos\left(\alpha_T^{(m)}-\gamma_T\right)+f_{R\max}\cos\left(\alpha_R^{(n)}-\gamma_R\right)\right]} \quad (14)$$

$$h_{pq}^{LoS}(t)=\sqrt{\frac{K_{pq}\Omega_{pq}}{1+K_{pq}}}e^{-j\frac{2\pi}{\lambda}D}\times e^{j\frac{\pi}{\lambda}\left[(L_t+1-2p)\delta_T\cos\theta_T+(L_r+1-2q)\delta_R\cos\left(\alpha_{Rq}^{LoS}-\theta_R\right)\right]}\times e^{j2\pi t f_{T\max}\cos\left(\pi-\alpha_{Rq}^{LoS}-\gamma_T\right)+j2\pi t f_{R\max}\cos\left(\alpha_{Rq}^{LoS}-\gamma_R\right)}. \quad (15)$$

The complex faded envelope in (1) also can be written as $h_{pq}(t)=h_{pq}^{(I)}(t)+jh_{pq}^{(Q)}(t)$, where

$$h_{pq}^{(I)}(t)=\Re\left\{h_{pq}^{SBT}(t)\right\}+\Re\left\{h_{pq}^{SBR}(t)\right\}+\Re\left\{h_{pq}^{DB}(t)\right\}+\Re\left\{h_{pq}^{LoS}(t)\right\} \quad (16)$$

$$h_{pq}^{(Q)}(t)=\Im\left\{h_{pq}^{SBT}(t)\right\}+\Im\left\{h_{pq}^{SBR}(t)\right\}+\Im\left\{h_{pq}^{DB}(t)\right\}+\Im\left\{h_{pq}^{LoS}(t)\right\} \quad (17)$$

are the in-phase (I) and quadrature (Q) components of the complex faded envelope, and $\Re\{\cdot\}$ and $\Im\{\cdot\}$ denote the real and imaginary operation, respectively.

III. Space-Time Correlation Functions and Space-Doppler Power Spectrum

Assuming a 2-D non-isotropic scattering environment, we now derive the closed-form space-time correlation function of the complex faded envelope in (1). We also show that this space-time correlation function reduces to the one derived in [9] if there are no single-bounced and LoS rays and 2-D isotropic scattering is assumed. Furthermore, we derive the space-time correlation functions of the I and Q components of the complex faded envelope for a 2-D isotropic scattering environment. Finally, we derive the space-Doppler power spectral density of the complex faded envelope, assuming a 2-D non-isotropic scattering environment.

The normalized space-time correlation function between two complex faded envelopes $h_{pq}(t)$ and $h_{\tilde{p}\tilde{q}}(t)$ is defined as

$$R_{pq,\tilde{p}\tilde{q}}(\delta_T,\delta_R,\tau)=\frac{\mathrm{E}\left[h_{pq}(t)h_{\tilde{p}\tilde{q}}(t+\tau)^*\right]}{\sqrt{\mathrm{E}\left[\left|h_{pq}(t)\right|^2\right]\mathrm{E}\left[\left|h_{\tilde{p}\tilde{q}}(t)\right|^2\right]}}$$
$$=\frac{\mathrm{E}\left[h_{pq}^{SBT}(t)h_{\tilde{p}\tilde{q}}^{SBT}(t+\tau)^*\right]}{\sqrt{\mathrm{E}\left[\left|h_{pq}^{SBT}(t)\right|^2\right]\mathrm{E}\left[\left|h_{\tilde{p}\tilde{q}}^{SBT}(t)\right|^2\right]}}+\frac{\mathrm{E}\left[h_{pq}^{DB}(t)h_{\tilde{p}\tilde{q}}^{DB}(t+\tau)^*\right]}{\sqrt{\mathrm{E}\left[\left|h_{pq}^{DB}(t)\right|^2\right]\mathrm{E}\left[\left|h_{\tilde{p}\tilde{q}}^{DB}(t)\right|^2\right]}}$$
$$+\frac{\mathrm{E}\left[h_{pq}^{SBR}(t)h_{\tilde{p}\tilde{q}}^{SBR}(t+\tau)^*\right]}{\sqrt{\mathrm{E}\left[\left|h_{pq}^{SBR}(t)\right|^2\right]\mathrm{E}\left[\left|h_{\tilde{p}\tilde{q}}^{SBR}(t)\right|^2\right]}}+\frac{\mathrm{E}\left[h_{pq}^{LoS}(t)h_{\tilde{p}\tilde{q}}^{LoS}(t+\tau)^*\right]}{\sqrt{\mathrm{E}\left[\left|h_{pq}^{LoS}(t)\right|^2\right]\mathrm{E}\left[\left|h_{\tilde{p}\tilde{q}}^{LoS}(t)\right|^2\right]}} \tag{18}$$

where $(\cdot)^*$ denotes complex conjugate operation, $\mathrm{E}[\cdot]$ is the statistical expectation operator, p, $\tilde{p}\in\{1,\ldots,L_t\}$, and q, $\tilde{q}\in\{1,\ldots,L_r\}$.

Using (12), (13), and (18), the space-time correlation functions of the single-bounced components can be written as

$$R_{pq,\tilde{p}\tilde{q}}^{SBT}(\delta_T,\delta_R,\tau)$$
$$=\frac{\mathrm{E}\left[h_{pq}^{SBT}(t)h_{\tilde{p}\tilde{q}}^{SBT}(t+\tau)^*\right]}{\sqrt{\mathrm{E}\left[\left|h_{pq}^{SBT}(t)\right|^2\right]\mathrm{E}\left[\left|h_{\tilde{p}\tilde{q}}^{SBT}(t)\right|^2\right]}}=\lim_{M\to\infty}\frac{\eta_T}{M}\sum_{m=1}^{M}$$
$$\times\mathrm{E}\left[e^{j\frac{2\pi}{\lambda}\left[(\tilde{p}-p)\delta_T\cos\left(\theta_T-\alpha_T^{(m)}\right)+(\tilde{q}-q)\delta_R\left(\Delta_T\sin\theta_R\sin\alpha_T^{(m)}-\cos\theta_R\right)\right]}\right.$$
$$\left.\times\,e^{-j2\pi\tau\left[f_{T\max}\cos\left(\alpha_T^{(m)}-\gamma_T\right)+f_{R\max}\left(\Delta_T\sin\gamma_R\sin\alpha_T^{(m)}-\cos\gamma_R\right)\right]}\right] \tag{19}$$

$$R_{pq,\tilde{p}\tilde{q}}^{SBR}(\delta_T,\delta_R,\tau)$$
$$=\frac{\mathrm{E}\left[h_{pq}^{SBR}(t)h_{\tilde{p}\tilde{q}}^{SBR}(t+\tau)^*\right]}{\sqrt{\mathrm{E}\left[\left|h_{pq}^{SBR}(t)\right|^2\right]\mathrm{E}\left[\left|h_{\tilde{p}\tilde{q}}^{SBR}(t)\right|^2\right]}}=\lim_{N\to\infty}\frac{\eta_R}{N}\sum_{n=1}^{N}$$
$$\times\mathrm{E}\left[e^{j\frac{2\pi}{\lambda}\left[(\tilde{q}-q)\delta_R\cos\left(\alpha_R^{(n)}-\theta_R\right)+(\tilde{p}-p)\delta_T\left(\Delta_R\sin\theta_T\sin\alpha_R^{(n)}+\cos\theta_T\right)\right]}\right.$$
$$\left.\times\,e^{-j2\pi\tau\left[f_{T\max}\left(\Delta_R\sin\gamma_T\sin\alpha_R^{(n)}+\cos\gamma_T\right)+f_{R\max}\cos\left(\alpha_R^{(n)}-\gamma_R\right)\right]}\right]. \tag{20}$$

Using (14) and (18), the space-time correlation function of the double-bounced component becomes

$$R_{pq,\tilde{p}\tilde{q}}^{DB}(\delta_T,\delta_R,\tau)$$
$$=\frac{\mathrm{E}\left[h_{pq}^{DB}(t)h_{\tilde{p}\tilde{q}}^{DB}(t+\tau)^*\right]}{\sqrt{\mathrm{E}\left[\left|h_{pq}^{DB}(t)\right|^2\right]\mathrm{E}\left[\left|h_{\tilde{p}\tilde{q}}^{DB}(t)\right|^2\right]}}=\lim_{M,N\to\infty}\frac{\eta_{TR}}{MN}\sum_{m=1}^{M}\sum_{n=1}^{N}$$
$$\times\,\mathrm{E}\left[e^{-j2\pi\tau\left(f_{T\max}\cos\left(\alpha_T^{(m)}-\gamma_T\right)+f_{R\max}\cos\left(\alpha_R^{(n)}-\gamma_R\right)\right)}\right.$$
$$\left.\times\,e^{j\frac{2\pi}{\lambda}\left[(\tilde{q}-q)\delta_R\cos\left(\alpha_R^{(n)}-\theta_R\right)+(\tilde{p}-p)\delta_T\cos\left(\theta_T-\alpha_T^{(m)}\right)\right]}\right]. \tag{21}$$

Since the number of local scatterers in the reference models described in Section II is infinite, the discrete AoDs, $\alpha_T^{(m)}$, and AoAs, $\alpha_R^{(n)}$, can be replaced with continuous random variables α_T and α_R with probability density functions (pdf) $f(\alpha_T)$ and $f(\alpha_R)$, respectively. Hence, the space-time correlation functions of the single- and double-bounced components can be rewritten as

$$R_{pq,\tilde{p}\tilde{q}}^{SBT}(\delta_T,\delta_R,\tau)=\eta_T\int_{-\pi}^{\pi}e^{j\frac{2\pi}{\lambda}(\tilde{p}-p)\delta_T\cos(\theta_T-\alpha_T)}$$
$$\times\,e^{-j2\pi\tau f_{T\max}\cos(\alpha_T-\gamma_T)}e^{j\frac{2\pi}{\lambda}(\tilde{q}-q)\delta_R(\Delta_T\sin\theta_R\sin\alpha_T-\cos\theta_R)}$$
$$\times\,e^{-j2\pi\tau f_{R\max}(\Delta_T\sin\gamma_R\sin\alpha_T-\cos\gamma_R)}f(\alpha_T)d\alpha_T \tag{22}$$

$$R_{pq,\tilde{p}\tilde{q}}^{SBR}(\delta_T,\delta_R,\tau)=\eta_R\int_{-\pi}^{\pi}e^{j\frac{2\pi}{\lambda}(\tilde{q}-q)\delta_R\cos(\alpha_R-\theta_R)}$$
$$\times\,e^{j\frac{2\pi}{\lambda}(\tilde{p}-p)\delta_T(\Delta_R\sin\theta_T\sin\alpha_R+\cos\theta_T)}e^{-j2\pi\tau f_{R\max}\cos(\alpha_R-\gamma_R)}$$
$$\times\,e^{-j2\pi\tau f_{T\max}(\Delta_R\sin\gamma_T\sin\alpha_R+\cos\gamma_T)}f(\alpha_R)d\alpha_R \tag{23}$$

$$R_{pq,\tilde{p}\tilde{q}}^{DB}(\delta_T,\delta_R,\tau)=\eta_{TR}\int_{-\pi}^{\pi}\int_{-\pi}^{\pi}f(\alpha_T)f(\alpha_R)$$
$$\times\,e^{-j2\pi\tau[f_{T\max}\cos(\alpha_T-\gamma_T)+f_{R\max}\cos(\alpha_R-\gamma_R)]}$$
$$\times\,e^{j\frac{2\pi}{\lambda}[(\tilde{p}-p)\delta_T\cos(\alpha_T-\theta_T)+(\tilde{q}-q)\delta_R\cos(\alpha_R-\theta_R)]}d\alpha_T d\alpha_R. \tag{24}$$

Prior work uses several different scatterer distributions, such as uniform [12], von Mises [13], Gaussian, and Laplacian [14]. In this section we use the von Mises pdf because it approximates many of the afore mentioned distributions (e.g., uniform and Gaussian), matches well measured results in [15], and in contrast to afore mentioned distributions, leads to closed-form solutions for many useful situations. The von Mises pdf is defined as [13]

$$f(\theta)\triangleq\frac{1}{2\pi I_0(k)}\exp\left[k\cos(\theta-\mu)\right] \tag{25}$$

where $\theta\in[-\pi,\pi)$, $I_0(\cdot)$ is the zeroth-order modified Bessel function of the first kind, $\mu\in[-\pi,\pi)$ is the mean angle at which the scatterers are distributed on the ring, and k controls the spread of scatterers around the mean. When $k=0$, $f(\theta)=1/(2\pi)$ is a uniform distribution yielding 2-D isotropic scattering. As k increases, the scatterers become more clustered around angle μ and the scattering becomes increasingly non-isotropic. By denoting the von Mises pdf for the $\mathrm{T_x}$ and $\mathrm{R_x}$ scatterers as $f(\alpha_T)=\exp\left[k_T\cos(\alpha_T-\mu_T)\right]/(2\pi I_0(k_T))$ and $f(\alpha_R)=\exp\left[k_R\cos(\alpha_R-\mu_R)\right]/(2\pi I_0(k_R))$, respectively, the space-time correlation functions of the single- and double-bounced components become, respectively

$$R_{pq,\tilde{p}\tilde{q}}^{SBT}(\delta_T,\delta_R,\tau)=\frac{\eta_T}{2\pi I_0(k_T)}\int_{-\pi}^{\pi}e^{j\frac{2\pi}{\lambda}(\tilde{p}-p)\delta_T\cos(\theta_T-\alpha_T)}$$
$$\times\,e^{j\frac{2\pi}{\lambda}(\tilde{q}-q)\delta_R(\Delta_T\sin\theta_R\sin\alpha_T-\cos\theta_R)}e^{k_T\cos(\alpha_T-\mu_T)}$$
$$\times\,e^{-j2\pi\tau[f_{T\max}\cos(\alpha_T-\gamma_T)+f_{R\max}(\Delta_T\sin\gamma_R\sin\alpha_T-\cos\gamma_R)]}d\alpha_T \tag{26}$$

$$R_{pq,\tilde{p}\tilde{q}}^{SBR}(\delta_T,\delta_R,\tau)=\frac{\eta_R}{2\pi I_0(k_R)}\int_{-\pi}^{\pi}e^{j\frac{2\pi}{\lambda}(\tilde{q}-q)\delta_R\cos(\alpha_R-\theta_R)}$$
$$\times\,e^{j\frac{2\pi}{\lambda}(\tilde{p}-p)\delta_T(\Delta_R\sin\theta_T\sin\alpha_R+\cos\theta_T)}e^{k_R\cos(\alpha_R-\mu_R)}$$
$$\times\,e^{-j2\pi\tau[f_{T\max}(\Delta_R\sin\gamma_T\sin\alpha_R+\cos\gamma_T)+f_{R\max}\cos(\alpha_R-\gamma_R)]}d\alpha_R \tag{27}$$

$$R^{DB}_{pq,\tilde{p}\tilde{q}}(\delta_T,\delta_R,\tau)=\frac{\eta_{TR}}{4\pi^2 I_0(k_T)I_0(k_R)}\int_{-\pi}^{\pi}\int_{-\pi}^{\pi}e^{k_T\cos(\alpha_T-\mu_T)}\times e^{k_R\cos(\alpha_R-\mu_R)}e^{j\frac{2\pi}{\lambda}[(\tilde{p}-p)\delta_T\cos(\alpha_T-\theta_T)+(\tilde{q}-q)\delta_R\cos(\alpha_R-\theta_R)]}\times e^{-j2\pi\tau[f_{T\max}\cos(\alpha_T-\gamma_T)+f_{R\max}\cos(\alpha_R-\gamma_R)]}d\alpha_T d\alpha_R. \quad (28)$$

Using trigonometric transformations, (26) and (27) become, respectively,

$$R^{SBT}_{pq,\tilde{p}\tilde{q}}(\delta_T,\delta_R,\tau)=\frac{\eta_T e^{-j\frac{2\pi}{\lambda}(\tilde{q}-q)\delta_R\cos\theta_R+j2\pi\tau f_{R\max}\cos\gamma_R}}{2\pi I_0(k_T)}\times\int_{-\pi}^{\pi}e^{x_{SBT}\cos\alpha_T+y_{SBT}\sin\alpha_T}d\alpha_T \quad (29)$$

$$R^{SBR}_{pq,\tilde{p}\tilde{q}}(\delta_T,\delta_R,\tau)=\frac{\eta_R e^{j\frac{2\pi}{\lambda}(\tilde{p}-p)\delta_T\cos\theta_T-j2\pi\tau f_{T\max}\cos\gamma_T}}{2\pi I_0(k_R)}\times\int_{-\pi}^{\pi}e^{x_{SBR}\cos\alpha_R+y_{SBR}\sin\alpha_R}d\alpha_R \quad (30)$$

where parameters x_{SBT}, y_{SBT}, x_{SBR}, and y_{SBR} are $x_{SBT}=j(2\pi/\lambda)(\tilde{p}-p)\delta_T\cos\theta_T-j2\pi\tau f_{T\max}\cos\gamma_T+k_T\cos\mu_T$, $y_{SBT}=j(2\pi/\lambda)((\tilde{p}-p)\delta_T\sin\theta_T+(\tilde{q}-q)\delta_R\Delta_T\sin\theta_R)-j2\pi\tau(f_{T\max}\sin\gamma_T+f_{R\max}\Delta_T\sin\gamma_R)+k_T\sin\mu_T$, $x_{SBR}=j(2\pi/\lambda)(\tilde{q}-q)\delta_R\cos\theta_R-j2\pi\tau f_{R\max}\cos\gamma_R+k_R\cos\mu_R$, and $y_{SBR}=j(2\pi/\lambda)((\tilde{p}-p)\delta_T\Delta_R\sin\theta_T+(\tilde{q}-q)\delta_R\sin\theta_R)-j2\pi\tau(f_{T\max}\Delta_R\sin\gamma_T+f_{R\max}\sin\gamma_R)+k_R\sin\mu_R$. Finally, using the equality $\int_{-\pi}^{\pi}e^{a\sin(c)+b\cos(c)}dc=2\pi I_0(\sqrt{a^2+b^2})$ [16, eq. 3.338–4], the space-time correlation functions of the single-bounced components become

$$R^{SBT}_{pq,\tilde{p}\tilde{q}}(\delta_T,\delta_R,\tau)=\eta_T e^{-j\frac{2\pi}{\lambda}(\tilde{q}-q)\delta_R\cos\theta_R+j2\pi\tau f_{R\max}\cos\gamma_R}\times\frac{I_0\left(\sqrt{x^2_{SBT}+y^2_{SBT}}\right)}{I_0(k_T)} \quad (31)$$

$$R^{SBR}_{pq,\tilde{p}\tilde{q}}(\delta_T,\delta_R,\tau)=\eta_R e^{j\frac{2\pi}{\lambda}(\tilde{p}-p)\delta_T\cos\theta_T-j2\pi\tau f_{T\max}\cos\gamma_T}\times\frac{I_0\left(\sqrt{x^2_{SBR}+y^2_{SBR}}\right)}{I_0(k_R)}. \quad (32)$$

Since α_T and α_R are independent random variables, the double integral in (28) reduces to the product of two single integrals. By grouping the terms in (28) into those containing α_T and those containing α_R, and by using trigonometric transformations and the equality [16, eq. 3.338–4], the space-time correlation function of the double-bounced component becomes

$$R^{DB}_{pq,\tilde{p}\tilde{q}}(\delta_T,\delta_R,\tau)=\eta_{TR}\frac{I_0\left(\sqrt{x^2_{DB}+y^2_{DB}}\right)I_0\left(\sqrt{z^2_{DB}+w^2_{DB}}\right)}{I_0(k_T)I_0(k_R)} \quad (33)$$

where parameters x_{DB}, y_{DB}, z_{DB}, and w_{DB} are $x_{DB}=j2\pi(\tilde{p}-p)\delta_T\cos\theta_T/\lambda-j2\pi\tau f_{T\max}\cos\gamma_T+k_T\cos\mu_T$, $y_{DB}=j2\pi(\tilde{p}-p)\delta_T\sin\theta_T/\lambda-j2\pi\tau f_{T\max}\sin\gamma_T+k_T\sin\mu_T$, $z_{DB}=j2\pi(\tilde{q}-q)\delta_R\cos\theta_R/\lambda-j2\pi\tau f_{R\max}\cos\gamma_R+k_R\cos\mu_R$, and $w_{DB}=j2\pi(\tilde{q}-q)\delta_R\sin\theta_R/\lambda-j2\pi\tau f_{R\max}\sin\gamma_R+k_R\sin\mu_R$, respectively.

Using (6) and (18), the space-time correlation function of the LoS component can be written as

$$R^{LoS}_{pq,\tilde{p}\tilde{q}}(\delta_T,\delta_R,\tau,t)=\sqrt{K_{pq}K_{\tilde{p}\tilde{q}}}e^{-j2\pi(\epsilon_{pq}-\epsilon_{\tilde{p}\tilde{q}})/\lambda}\times e^{-j2\pi\tau\left[f_{T\max}\cos\left(\pi-\alpha^{LoS}_{R\tilde{q}}-\gamma_T\right)+f_{R\max}\cos\left(\alpha^{LoS}_{R\tilde{q}}-\gamma_R\right)\right]}\times e^{j2\pi t f_{T\max}\left[\cos\left(\pi-\alpha^{LoS}_{Rq}-\gamma_T\right)-\cos\left(\pi-\alpha^{LoS}_{R\tilde{q}}-\gamma_T\right)\right]}\times e^{j2\pi t f_{R\max}\left[\cos\left(\alpha^{LoS}_{Rq}-\gamma_R\right)-\cos\left(\alpha^{LoS}_{R\tilde{q}}-\gamma_R\right)\right]}. \quad (34)$$

Based on the assumption $\max\{R_t,R_r\}\ll D$, from Fig. 2 we obtain $\alpha^{LoS}_{Rq}=\alpha^{LoS}_{R\tilde{q}}\approx\pi$ which in turn simplifies (34) to

$$R^{LoS}_{pq,\tilde{p}\tilde{q}}(\delta_T,\delta_R,\tau)\approx\sqrt{K_{pq}K_{\tilde{p}\tilde{q}}}e^{j\frac{2\pi}{\lambda}\delta_T\cos\theta_T-j\frac{2\pi}{\lambda}\delta_R\cos\theta_R}\times e^{j2\pi\tau f_{T\max}\cos\gamma_T-j2\pi\tau f_{R\max}\cos\gamma_R}. \quad (35)$$

Finally, the normalized space-time correlation function $R_{pq,\tilde{p}\tilde{q}}(\delta_T,\delta_R,\tau)$ between two complex faded envelopes $h_{pq}(t)$ and $h_{\tilde{p}\tilde{q}}(t)$ becomes a summation of the normalized space-time correlation functions $R^{SBT}_{pq,\tilde{p}\tilde{q}}(\delta_T,\delta_R,\tau)$, $R^{SBR}_{pq,\tilde{p}\tilde{q}}(\delta_T,\delta_R,\tau)$, $R^{DB}_{pq,\tilde{p}\tilde{q}}(\delta_T,\delta_R,\tau)$, and $R^{LoS}_{pq,\tilde{p}\tilde{q}}(\delta_T,\delta_R,\tau)$, defined in (31)–(33) and (35), respectively.

Many existing correlation functions are special cases of the MIMO M-to-M space-time correlation function in (18). The simplest special case of (18) is Clarke's temporal correlation function $J_0(2\pi f_{R\max}\tau)$ [17], obtained for $K=0$ (NLoS condition), $k_R=0$ (2-D isotropic scattering around $\mathrm{R_x}$), $f_{T\max}=0$, $k_T=0$, $\eta_T=0$, $\eta_{TR}=0$ (fixed $\mathrm{T_x}$, no scattering around $\mathrm{T_x}$), and $\delta_T=\delta_R=0$ (single-antenna $\mathrm{T_x}$ and $\mathrm{R_x}$), where $J_0(\cdot)$ is the first kind zeroth-order Bessel function. Expressions for other space-time correlation functions based on the "one-ring" model [18], [19] can be similarly obtained. The temporal correlation function for M-to-M channels, assuming 2-D isotropic scattering, $J_0(2\pi f_{T\max}\tau)J_0(2\pi f_{R\max}\tau)$ [1] is obtained for $K=0$, $\eta_T=\eta_R=0$, $k_T=k_R=0$, and $\delta_T=\delta_R=0$. Similarly, the spatial correlation function for M-to-M channels $J_0(2\pi(\tilde{p}-p)\delta_T/\lambda)J_0(2\pi(\tilde{q}-q)\delta_R/\lambda)$ [20] is obtained for $K=0$, $\eta_T=\eta_R=0$, $k_T=k_R=0$, and $\tau=0$. Finally, the space-time correlation function for M-to-M channels, assuming 2-D isotropic scattering, $J_0(\sqrt{x^2_{DB}+y^2_{DB}})J_0(\sqrt{z^2_{DB}+w^2_{DB}})$ [9] is obtained for $K=0$, $\eta_T=\eta_R=0$, and $k_T=k_R=0$.

The space-time correlation functions of the I and Q components of the complex faded envelope can be obtained by substituting (16) and (17) into (18). Using similar derivations as above, it can be shown that for a large number of scatterers ($M,\ N\to\infty$) and 2-D isotropic scattering the space-time correlation functions of the I and Q components of the complex faded envelope are

$$\begin{aligned}R^{(I/Q,I/Q)}_{pq,\tilde{p}\tilde{q}}(\delta_T,\delta_R,\tau)&=\Re\left\{R_{pq,\tilde{p}\tilde{q}}(\delta_T,\delta_R,\tau)\right\}\\&=\eta_T\cos\left(2\pi\tau f_{R\max}\cos\gamma_R-2\pi(\tilde{q}-q)(\delta_R/\lambda)\cos\theta_R\right)\\&\quad\times J_0\left(\sqrt{x^2_{iSBT}+y^2_{iSBT}}\right)+\eta_R\\&\quad\times\cos\left(2\pi(\tilde{p}-p)(\delta_T/\lambda)\cos\theta_T-2\pi\tau f_{T\max}\cos\gamma_T\right)\\&\quad\times J_0\left(\sqrt{x^2_{iSBR}+y^2_{iSBR}}\right)+\eta_{TR}J_0\left(\sqrt{x^2_{iDB}+y^2_{iDB}}\right)\end{aligned}$$

$$\times J_0\left(\sqrt{z_{iDB}^2+w_{iDB}^2}\right)+\sqrt{K_{pq}K_{\tilde{p}\tilde{q}}}$$
$$\times\cos\left[2\pi(\delta_T/\lambda)\cos\theta_T-2\pi(\delta_R/\lambda)\cos\theta_R + 2\pi\tau f_{T\max}\cos\gamma_T-2\pi\tau f_{R\max}\cos\gamma_R\right] \quad (36)$$

$$R_{pq,\tilde{p}\tilde{q}}^{(I,Q)}(\delta_T,\delta_R,\tau)=\Im\left\{R_{pq,\tilde{p}\tilde{q}}(\delta_T,\delta_R,\tau)\right\}$$
$$=\eta_T\sin\left(2\pi\tau f_{R\max}\cos\gamma_R-2\pi(\tilde{q}-q)(\delta_R/\lambda)\cos\theta_R\right)$$
$$\times J_0\left(\sqrt{x_{iSBT}^2+y_{iSBT}^2}\right)+\eta_R$$
$$\times\sin\left(2\pi(\tilde{p}-p)(\delta_T/\lambda)\cos\theta_T-2\pi\tau f_{T\max}\cos\gamma_T\right)$$
$$\times J_0\left(\sqrt{x_{iSBR}^2+y_{iSBR}^2}\right)+\sqrt{K_{pq}K_{\tilde{p}\tilde{q}}}$$
$$\times\sin\left[2\pi(\delta_T/\lambda)\cos\theta_T-2\pi(\delta_R/\lambda)\cos\theta_R + 2\pi\tau f_{T\max}\cos\gamma_T-2\pi\tau f_{R\max}\cos\gamma_R\right] \quad (37)$$

where parameters y_{iSBT}, y_{iSBR}, x_{iSBT}, x_{iSBR}, x_{iDB}, y_{iDB}, z_{iDB}, and w_{iDB} are equal to $y_{iSBT}=2\pi[(\tilde{p}-p)(\delta_T/\lambda)\times\sin\theta_T+(\tilde{q}-q)(\delta_R/\lambda)\Delta_T\sin\theta_R-\tau(f_{T\max}\sin\gamma_T+f_{R\max}\Delta_T\sin\gamma_R)]$, $y_{iSBR}=2\pi[((\tilde{q}-q)(\delta_R/\lambda)\sin\theta_R+(\tilde{p}-p)(\delta_T/\lambda)\Delta_R\sin\theta_T)-\tau(f_{T\max}\Delta_R\sin\gamma_T+f_{R\max}\sin\gamma_R)]$, $x_{iSBT}=2\pi[(\tilde{p}-p)(\delta_T/\lambda)\cos\theta_T-\tau f_{T\max}\cos\gamma_T]$, $x_{iSBR}=2\pi[(\tilde{q}-q)(\delta_R/\lambda)\cos\theta_R-\tau f_{R\max}\cos\gamma_R]$, $x_{iDB}=2\pi[(\tilde{p}-p)(\delta_T/\lambda)\cos\theta_T-\tau f_{T\max}\cos\gamma_T]$, $y_{iDB}=2\pi[(\tilde{p}-p)(\delta_T/\lambda)\sin\theta_T-\tau f_{T\max}\sin\gamma_T]$, $z_{iDB}=2\pi[(\tilde{q}-q)(\delta_R/\lambda)\cos\theta_R-\tau f_{R\max}\cos\gamma_R]$, $w_{iDB}=2\pi[(\tilde{q}-q)(\delta_R/\lambda)\sin\theta_R-\tau f_{R\max}\sin\gamma_R]$. The derivations are omitted for brevity.

The space-Doppler power spectral density (sD-psd) of the complex faded envelope is the Fourier transformation of the space-time correlation function. We start the derivation for the sD-psds of the single-bounced components by noting that the functions $I_0(\sqrt{x_{SBT}^2+y_{SBT}^2})$ and $I_0(\sqrt{x_{SBR}^2+y_{SBR}^2})$ can be written as

$$I_0\left[j2\pi f_{T\max}\times\sqrt{(\tau A_{SBT})^2+\left(\frac{p_{x_{SBT}}q_{y_{SBT}}}{f_{T\max}}-\frac{p_{y_{SBT}}q_{x_{SBT}}}{f_{T\max}}+\frac{w_{y_{SBT}}}{2\pi f_{T\max}}\right)^2}\right] \quad (38)$$

$$I_0\left[j2\pi f_{R\max}\times\sqrt{(\tau-A_{SBR})^2+\left(\frac{p_{x_{SBR}}q_{y_{SBR}}}{f_{R\max}}-\frac{p_{y_{SBR}}q_{x_{SBR}}}{f_{R\max}}+\frac{w_{y_{SBR}}}{2\pi f_{R\max}}\right)^2}\right] \quad (39)$$

where $p_{x_{SBT}}=(\tilde{p}-p)(\delta_T/\lambda)\cos\theta_T$, $q_{x_{SBT}}=\cos\gamma_T$, $A_{SBT}=(2\pi p_{x_{SBT}}q_{x_{SBT}}+2\pi p_{y_{SBT}}q_{y_{SBT}}+w_{x,SBT})/2\pi f_{T\max}$, $p_{y_{SBT}}=[(\tilde{p}-p)\delta_T\sin\theta_T+(\tilde{q}-q)\delta_R\Delta_T\sin\theta_R]/\lambda$, $q_{y_{SBT}}\approx\sin\gamma_T$, $A_{SBR}=(2\pi p_{x_{SBR}}q_{x_{SBR}}+2\pi p_{y_{SBR}}q_{y_{SBR}}+w_{x_{SBR}})/2\pi f_{R\max}$, $w_{x_{SBT}}=-jk_T\cos(\gamma_T-\mu_T)$, $w_{y_{SBT}}=-jk_T\sin(\gamma_T-\mu_T)$, $p_{x_{SBR}}=(\tilde{q}-q)(\delta_R/\lambda)\cos\theta_R$, $q_{x_{SBR}}=\cos\gamma_R$, $w_{x_{SBR}}=-jk_R\cos(\gamma_R-\mu_R)$, $p_{y_{SBR}}=[(\tilde{p}-p)\times\delta_T\Delta_R\sin\theta_T+(\tilde{q}-q)\delta_R\sin\theta_R]/\lambda$, $q_{y_{SBR}}\approx\sin\gamma_R$, and $w_{y_{SBR}}=-jk_R\sin(\gamma_R-\mu_R)$. Using (38), (39), and equality $\int_0^\infty I_0(\alpha\sqrt{t^2+u^2})\cos(\beta t)dt=\cosh(u\sqrt{\alpha^2-\beta^2})/\sqrt{\alpha^2-\beta^2}$ [16, eq. 6.677–3], the sD-psds of the single-bounced components become

$$\mathcal{F}\left\{R_{pq,\tilde{p}\tilde{q}}^{SBT}(\delta_T,\delta_R,\tau)\right\}=\frac{\eta_T}{I_0(k_T)}\times\frac{\exp\{-j2\pi p_{x_{SBR}}-j2\pi(f-f_{R\max}\cos\gamma_R)A_{SBT}\}}{\pi f_{T\max}\sqrt{1-\left[(f-f_{R\max}\cos\gamma_R)/f_{T\max}\right]^2}}$$
$$\times\cosh\left[\left(k_T\sin(\mu_T-\gamma_T)+j2\pi p_{x_{SBT}}q_{y_{SBT}}-j2\pi p_{y_{SBT}}q_{x_{SBT}}\right)\times\sqrt{1-\left[(f-f_{R\max}\cos\gamma_R)/f_{T\max}\right]^2}\right] \quad (40)$$

$$\mathcal{F}\left\{R_{pq,\tilde{p}\tilde{q}}^{SBR}(\delta_T,\delta_R,\tau)\right\}=\frac{\eta_R}{I_0(k_R)}\times\frac{\exp\{j2\pi p_{x_{SBT}}-j2\pi(f+f_{T\max}\cos\gamma_T)A_{SBR}\}}{\pi f_{R\max}\sqrt{1-\left[(f+f_{T\max}\cos\gamma_T)/f_{R\max}\right]^2}}$$
$$\times\cosh\left[\left(k_R\sin(\mu_R-\gamma_R)+j2\pi p_{x_{SBR}}q_{y_{SBR}}-j2\pi p_{y_{SBR}}q_{x_{SBR}}\right)\times\sqrt{1-\left[(f+f_{T\max}\cos\gamma_T)/f_{R\max}\right]^2}\right] \quad (41)$$

where $\cosh(\cdot)$ is the hyperbolic cosine, $|f-f_{R\max}\cos\gamma_R|\le f_{T\max}$ and $|f+f_{T\max}\cos\gamma_T|\le f_{R\max}$.

Note that existing power spectral densities derived assuming "one-ring" model, are special cases of (41). The simplest special case of (41) is Clarke's power spectrum $1/(\pi\sqrt{f_{R\max}^2-f^2})$, $|f|\le f_{R\max}$ [17], obtained for $k_R=0$ (2-D isotropic scattering around $\mathrm{R_x}$), $f_{T\max}=0$, $k_T=0$ (fixed $\mathrm{T_x}$, no scattering around $\mathrm{T_x}$), and $\delta_T=\delta_R=0$ (single-antenna $\mathrm{T_x}$ and $\mathrm{R_x}$). Similarly, the 2-D non-isotropic power spectral density in (3) of [13] is obtained for $f_{T\max}=0$ and $\delta_T=\delta_R=0$.

We start the derivation for the sD-psd of the double-bounced component by noting that

$$\mathcal{F}\left\{I_0\left(\sqrt{x_{DB}^2+y_{DB}^2}\right)I_0\left(\sqrt{z_{DB}^2+w_{DB}^2}\right)\right\}=\mathcal{F}\left\{I_0\left(\sqrt{x_{DB}^2+y_{DB}^2}\right)\right\}\odot\mathcal{F}\left\{I_0\left(\sqrt{z_{DB}^2+w_{DB}^2}\right)\right\} \quad (42)$$

where $\odot$ denotes convolution. Using (42) and similar reasoning as above, the sD-psd of the double-bounced component becomes

$$\mathcal{F}\left\{R_{pq,\tilde{p}\tilde{q}}^{DB}(\delta_T,\delta_R,\tau)\right\}=\frac{\eta_{TR}}{I_0(k_T)\pi f_{T\max}\sqrt{1-(f/f_{T\max})^2}}\times e^{-j(2\pi p_{x_{DB}}q_{x_{DB}}+2\pi p_{y_{DB}}q_{y_{DB}}+jk_T\cos(\gamma_T-\mu_T))f/f_{T\max}}$$
$$\times\cosh\left[\left(k_T\sin(\mu_T-\gamma_T)+j2\pi p_{x_{DB}}q_{y_{DB}}-j2\pi p_{y_{DB}}q_{x_{DB}}\right)\times\sqrt{1-(f/f_{T\,rmmax})^2}\right]$$
$$\odot\frac{e^{-j(2\pi p_{z_{DB}}q_{z_{DB}}+2\pi p_{w_{DB}}q_{w_{DB}}+jk_R\cos(\gamma_R-\mu_R))f/f_{R\max}}}{I_0(k_R)\pi f_{R\max}\sqrt{1-(f/f_{R\max})^2}}$$
$$\times\cosh\left[\left(k_R\sin(\mu_R-\gamma_R)+j2\pi p_{z_{DB}}q_{w_{DB}}-j2\pi p_{w_{DB}}q_{z_{DB}}\right)\times\sqrt{1-(f/f_{R\max})^2}\right] \quad (43)$$

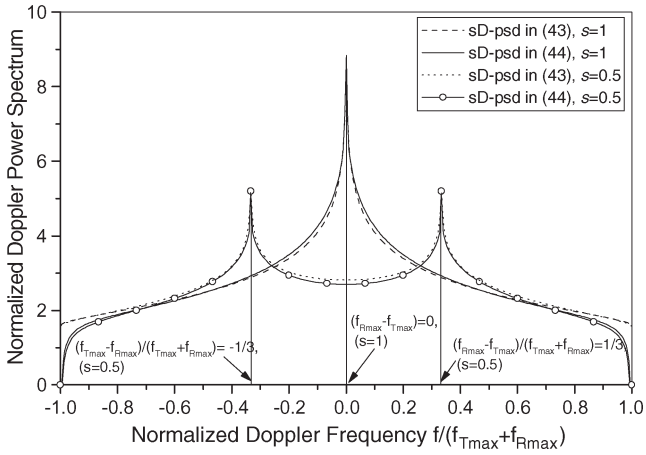

Fig. 3. Comparison of the normalized Doppler power spectra in (43) and (44) for $\delta_T = \delta_R = 0$ and different rations $s = f_{R\max}/f_{T\max}$.

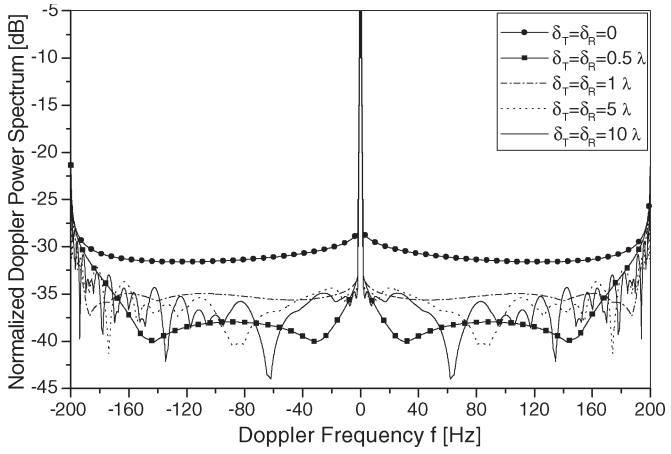

Fig. 4. Normalized space-Doppler power spectra characteristic for the outdoor M-to-M micro-cells. The curves are obtained with parameters $s = f_{R\max}/f_{T\max} = 1, \theta_T = \pi/3, \theta_R = \pi/4, \gamma_T = \gamma_R = \pi/2, \eta_T = \eta_R = 0.4, \eta_{TR} = 0.2, k_T = k_R = 0, K = 10$, and $L_t = L_r = 2$.

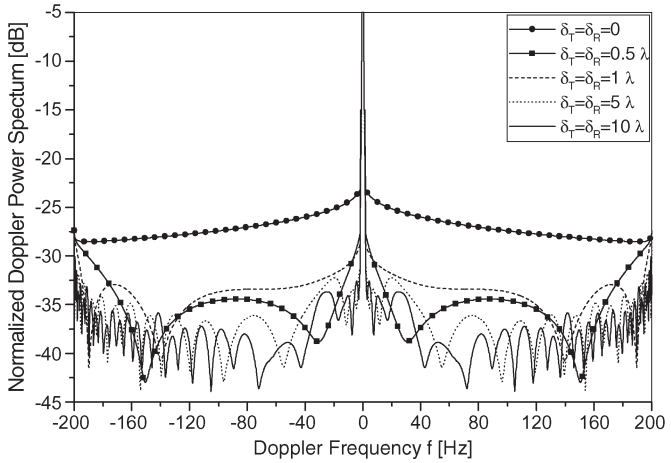

Fig. 5. Normalized space-Doppler power spectra characteristic for the outdoor M-to-M macro-cells. The curves are obtained with parameters $s = f_{R\max}/f_{T\max} = 1, \theta_T = \pi/3, \theta_R = \pi/4, \gamma_T = \gamma_R = \pi/2, \eta_T = \eta_R = 0.1, \eta_{TR} = 0.8, k_T = k_R = 0, K = 10$, and $L_t = L_r = 2$.

where $p_{x_{DB}} = (\tilde{p} - p)(\delta_T/\lambda)\cos\theta_T$, $q_{x_{SBT}} = \cos\gamma_T$, $p_{y_{DB}} = (\tilde{p} - p)(\delta_T/\lambda)\sin\theta_T$, $q_{y_{SBT}} = \sin\gamma_T$, $p_{z_{DB}} = (\tilde{q} - q)(\delta_R/\lambda)\cos\theta_R$, $q_{z_{DB}} = \cos\gamma_R$, $p_{w_{DB}} = (\tilde{q} - q)(\delta_R/\lambda)\sin\theta_R$, $q_{w_{DB}} = \sin\gamma_R$, and $|f| \leq f_{T\max} + f_{R\max}$.

For 2-D isotropic scattering and $\delta_T = \delta_R = 0$ (SISO system), the sD-psd of the double-bounced component has the closed-form expression [1]

$$\mathcal{F}\left\{R^{DB}_{pq,\tilde{p}\tilde{q}}(0,0,\tau)\right\} = \frac{1}{\pi^2\sqrt{s}f_{T\max}} \times K\left[\frac{1+s}{2\sqrt{s}}\sqrt{1-\left(\frac{f}{(1+s)f_{T\max}}\right)^2}\right] \quad (44)$$

where $K[\cdot]$ is the complete elliptic integral of the first kind and s is the ratio of the maximum Doppler frequencies $f_{R\max}$ and $f_{T\max}$, i.e., $s = f_{R\max}/f_{T\max}$. To validate the derived sD-psd in (43), we compare this expression for 2-D isotropic scattering and $\delta_T = \delta_R = \gamma_T = \gamma_R = 0$ with the sD-psd in (44). For different ratios $s = f_{R\max}/f_{T\max}$, Fig. 3 shows good agreement between the sD-psds in (43) and (44).

By calculating the Fourier transformation of the space-time correlation function in (35), we obtain the space-Doppler power spectral density of the LoS component

$$\mathcal{F}\left\{R^{LoS}_{pq,\tilde{p}\tilde{q}}(\delta_T,\delta_R,\tau)\right\} = \sqrt{K_{pq}K_{\tilde{p}\tilde{q}}}e^{j\frac{2\pi}{\lambda}[(\tilde{p}-p)\delta_T\cos\theta_T - (\tilde{q}-q)\delta_R\cos\theta_R]} \times \delta(f - f_{T\max}\cos\gamma_T + f_{R\max}\cos\gamma_R) \quad (45)$$

where $\delta(\cdot)$ denotes the Dirac delta function.

Finally, the sD-psd $S_{pq,\tilde{p}\tilde{q}}(\delta_T,\delta_R,f)$ between two complex faded envelopes $h_{pq}(t)$ and $h_{\tilde{p}\tilde{q}}(t)$ becomes a summation of the sD-psds $S^{SBT}_{pq,\tilde{p}\tilde{q}}(\delta_T,\delta_R,f)$, $S^{SBR}_{pq,\tilde{p}\tilde{q}}(\delta_T,\delta_R,f)$, $S^{DB}_{pq,\tilde{p}\tilde{q}}(\delta_T,\delta_R,f)$, and $S^{LoS}_{pq,\tilde{p}\tilde{q}}(\delta_T,\delta_R,f)$, defined as in (40), (41), (43), and (45), respectively.

In Figs. 4 and 5, we plot the sD-psd, $S_{pq,\tilde{p}\tilde{q}}(\delta_T,\delta_R,f)$, for several MIMO systems with parameters $s = f_{R\max}/f_{T\max} = 1$, $\delta_T = \delta_R \in \{0.5\lambda,\ 1\lambda,\ 5\lambda,\ 10\lambda\}$, $\theta_T = \pi/3$, $\theta_R = \pi/4$, $\gamma_T = \gamma_R = \pi/2$, and $L_t = L_r = 2$. In these figures, we analyze the radio propagation in outdoor micro- and macro-cells, assuming 2-D isotropic scattering ($k_T = k_R = 0$) and line-of-sight ($K = 10$) conditions between the transmitter and receiver. In Fig. 4, we assume that the single-bounced rays bear more energy than the double-bounced rays, i.e., $\eta_T = \eta_R = 0.4$ and $\eta_{TR} = 0.2$, which is characteristic of outdoor micro-cell propagation. We can observe that this spectrum is similar to the U-shaped spectrum of F-to-M cellular channels. In Fig. 5, we consider the macro-cell propagation, i.e. the double-bounced rays bear more energy than the single-bounced rays ($\eta_T = \eta_R = 0.1$ and $\eta_{TR} = 0.8$). In this case, the sD-psd differs from the U-shaped spectrum of cellular channels. Finally, our theoretical Doppler spectra closely match the measured Doppler spectra in [6] and [7].

IV. MIMO Mobile-to-Mobile Simulation Models

The reference models for MIMO M-to-M channels described in [9] and Section II assume an infinite number of scatterers, which prevents practical implementation. It is desirable to design simulation models with a finite number of scatterers, while still matching the statistical properties of the reference models.

A. MMEDS Model

Hogstad *et al.* [10] were the first to propose a deterministic MIMO M-to-M sum-of-sinusoids (SoS) model called the Modified Method of Exact Doppler Spreads (MMEDS). The MMEDS model describes radio propagation in outdoor macro-cells by assuming that all rays are double-bounced. By choosing only the phases to be random variables, the statistical properties of this model converge to those of the reference model in a single simulation trial. Using the reference model in [9] and assuming 2-D scattering, they defined the received complex faded envelope as

$$h_{pq}(t) = \sum_{m,n=1}^{M,N} \frac{a_{p,m}c_{m,n}b_{n,q}}{\sqrt{MN}} \times e^{j\left[2\pi f_{R\max}t\cos(\alpha_T^{(m)}-\gamma_T)+2\pi f_{R\max}t\cos(\alpha_R^{(n)}-\gamma_R)+\phi_{mn}\right]} \quad (46)$$

where $a_{p,m} = \exp\{j\pi(L_t+1-2p)\delta_T\cos(\alpha_T^{(m)}-\theta_T)/\lambda\}$, $c_{m,n} = \exp\{j2\pi(R_t\cos\alpha_T^{(m)} - R_r\cos\alpha_R^{(n)})/\lambda\}$, $b_{n,q} = \exp\{j\pi(L_r+1-2q)\delta_R\cos(\alpha_R^{(n)}-\theta_R)/\lambda\}$, and parameters p and q take values from the sets $p\in\{1,\ldots,L_t\}$ and $q\in\{1,\ldots,L_r\}$, respectively. The parameters θ_T, θ_R, γ_T, γ_R, $f_{T\max}$, and $f_{R\max}$ are defined as in Section II. With the MMEDS model, the phases ϕ_{mn} are independent random variables uniformly distributed on the interval $[0,2\pi)$, and the angles of departure $\alpha_T^{(m)}$ and the angles of arrivals $\alpha_R^{(n)}$ are chosen as follows:

$$\alpha_T^{(m)} = \frac{2\pi}{M}(m-0.5)+\gamma_T \quad (47)$$

$$\alpha_R^{(n)} = \frac{2\pi}{N}(n-0.5)+\gamma_R \quad (48)$$

for $m=1,\ldots,M$, $n=1,\ldots,N$, respectively.

As we will show, the MMEDS model has the disadvantage that the statistical properties match those of the reference model only for a small range of normalized time delays ($0\le f_{T\max}T_s\le 5$). Furthermore, the model requires large number of scatterers (i.e., M, $N=40$) to match statistical properties of the reference model. Finally, the MMEDS model assumes that all rays in outdoor macro-cells are double-bounced, which is not always the case.

B. New Simulation Models

In this section, we propose more general simulation models that describe propagation in outdoor micro- and macro-cells. In our models, the complex faded envelope is designed as a superposition of the LoS, the single-bounced, and the double-bounced rays. Assuming 2-D isotropic scattering and using the reference model described in Section II, we propose the following function as a received complex faded envelope: $h_{pq}(t) = h_{pq}^{(I)}(t) + jh_{pq}^{(Q)}(t)$, where

$$\begin{aligned}h_{pq}^{(I)}(t) =& \sum_{m=1}^{M}\frac{2P_T}{\sqrt{M}}\cos[\beta_m - K_q\cos\theta_R - 2\pi t f_{R\max}\cos\gamma_R]\\ &\times\cos\Big[K_p\cos\Big(\theta_T-\alpha_T^{(m)}\Big)+2\pi t f_{T\max}\\ &\times\cos\Big(\alpha_T^{(m)}-\gamma_T\Big)+K_q\Delta_T\sin\theta_R\sin\alpha_T^{(m)}\\ &+2\pi t f_{R\max}\Delta_T\sin\gamma_R\sin\alpha_T^{(m)}+\phi_m\Big]\\ &+\sum_{n=1}^{N}\frac{2P_R}{\sqrt{N}}\cos[\beta_n+K_p\cos\theta_T+2\pi t f_{T\max}\cos\gamma_T]\\ &\times\cos\Big[K_q\cos\Big(\alpha_R^{(n)}-\theta_R\Big)+2\pi t f_{R\max}\\ &\times\cos\Big(\alpha_R^{(n)}-\gamma_R\Big)+K_p\Delta_R\sin\theta_T\sin\alpha_R^{(n)}\\ &+2\pi t f_{T\max}\Delta_R\sin\gamma_T\sin\alpha_R^{(n)}+\phi_n\Big]\\ &+\sum_{m,n=1}^{M,N}\frac{2P_{TR}}{\sqrt{MN}}\cos\Big[K_p\cos\Big(\theta_T-\alpha_T^{(m)}\Big)\\ &+2\pi t f_{T\max}\cos\Big(\alpha_T^{(m)}-\gamma_T\Big)\Big]\\ &\times\cos\Big[K_q\cos\Big(\alpha_R^{(n)}-\theta_R\Big)+2\pi t f_{R\max}\\ &\times\cos\Big(\alpha_R^{(n)}-\gamma_R\Big)+\phi_{mn}\Big]\\ &+P_{LoS}\cos\big[K_p\cos\theta_T+K_q\cos\big(\alpha_{Rq}^{LoS}\theta_R\big)\\ &+2\pi t\left(f_T^{LoS}+f_R^{LoS}\right)\big]\end{aligned} \quad (49)$$

$$\begin{aligned}h_{pq}^{(Q)}(t) =& \sum_{m=1}^{M}\frac{2P_T}{\sqrt{M}}\sin[\beta_m - K_q\cos\theta_R - 2\pi t f_{R\max}\cos\gamma_R]\\ &\times\cos\Big[K_p\sin\Big(\theta_T-\alpha_T^{(m)}\Big)+2\pi t f_{T\max}\\ &\times\sin\Big(\alpha_T^{(m)}-\gamma_T\Big)+K_q\Delta_T\sin\theta_R\cos\alpha_T^{(m)}\\ &+2\pi t f_{R\max}\Delta_T\sin\gamma_R\cos\alpha_T^{(m)}+\phi_m\Big]\\ &+\sum_{n=1}^{N}\frac{2P_R}{\sqrt{N}}\sin[\beta_n+K_p\cos\theta_T+2\pi t f_{T\max}\cos\gamma_T]\\ &\times\cos\Big[K_q\sin\Big(\alpha_R^{(n)}-\theta_R\Big)+2\pi t f_{R\max}\\ &\times\sin\Big(\alpha_R^{(n)}-\gamma_R\Big)+K_p\Delta_R\sin\theta_T\cos\alpha_R^{(n)}\\ &+2\pi t f_{T\max}\Delta_R\sin\gamma_T\cos\alpha_R^{(n)}+\phi_n\Big]\\ &+\sum_{m,n=1}^{M,N}\frac{2P_{TR}}{\sqrt{MN}}\sin\Big[K_p\cos\Big(\theta_T-\alpha_T^{(m)}\Big)\\ &+2\pi t f_{T\max}\cos\Big(\alpha_T^{(m)}-\gamma_T\Big)\Big]\\ &\times\sin\Big[K_q\sin\Big(\alpha_R^{(n)}-\theta_R\Big)+2\pi t f_{R\max}\\ &\times\sin\Big(\alpha_R^{(n)}-\gamma_R\Big)+\phi_{mn}\Big]\\ &+P_{LoS}\sin\big[K_p\cos\theta_T+K_q\cos\big(\alpha_{Rq}^{LoS}-\theta_R\big)\\ &+2\pi t\left(f_T^{LoS}+f_R^{LoS}\right)\big]\end{aligned} \quad (50)$$

are the in-phase (I) and quadrature (Q) components of the complex faded envelope, β_m and β_n are the random path gains, $P_T=\sqrt{\eta_T\Omega_{pq}/(K_{pq}+1)}$, $P_R=\sqrt{\eta_R\Omega_{pq}/(K_{pq}+1)}$, $P_{TR}=\sqrt{\eta_{TR}\Omega_{pq}/(K_{pq}+1)}$, $K_q=2\pi(0.5L_r+0.5-q)\delta_R/\lambda$, $P_{LoS}=\sqrt{K_{pq}\Omega_{pq}/(1+K_{pq})}$, $K_p=2\pi(0.5L_t+0.5-p)\delta_T/\lambda$, $f_T^{LoS}=f_{T\max}\cos(\pi-\alpha_{Rq}^{LoS}-\gamma_T)$ and $f_R^{LoS}=f_{R\max}\cos(\alpha_{Rq}^{LoS}-\gamma_R)$.

The I and Q components in (49) and (50) are constructed as follows: the single-bounced components of the complex faded envelope are constructed using a similar method to one

proposed in [21] for the SISO F-to-M model, whereas the double-bounced components of the complex faded envelope are constructed using a similar method to one proposed in [5] for the SISO M-to-M model.

We first propose an ergodic statistical (deterministic) model, which needs only one simulation trial to obtain the desired statistical properties. The complex faded envelope is $h_{pq}(t) = h_{pq}^{(I)}(t) + jh_{pq}^{(Q)}(t)$, where functions $h_{pq}^{(I)}(t)$ and $h_{pq}^{(Q)}(t)$ are defined in (49) and (50). For this model, the phases ϕ_{mn} are generated as independent random variables uniformly distributed on the interval $[-\pi, \pi)$. The AoDs, AoAs and random path gains are chosen as follows:

$$\alpha_T^{(m)} = \frac{\pi}{M}(m - 0.5) + \gamma_T \tag{51}$$

$$\alpha_R^{(n)} = \frac{2\pi}{N}(n - 0.5) + \gamma_R \tag{52}$$

$$\beta_m = \frac{\pi(m - 0.5)}{M} \tag{53}$$

$$\beta_n = \frac{2\pi(n - 0.5)}{N} \tag{54}$$

for $m = 1, \ldots, M$, $n = 1, \ldots, N$, respectively. Note that the AoDs, AoAs, and random path gains differ from those in [21]. For M, $N \to \infty$, our deterministic model can be shown to exhibit properties (36) and (37) of the reference model. Derivations are omitted for brevity.

By allowing amplitudes, phases, and Doppler frequencies to be random variables, our deterministic model can be modified to match statistical properties of the reference model over a wider range of normalized time delays, while at the same time requiring a smaller number of scatterers around the $\mathrm{T_x}$ and $\mathrm{R_x}$. The statistical properties of this model vary for each simulation trial, but will converge to desired ensemble averaged properties when averaged over a sufficient number of simulation trials.

The complex faded envelope is $h_{pq}(t) = h_{pq}^{(I)}(t) + jh_{pq}^{(Q)}(t)$, where functions $h_{pq}^{(I)}(t)$ and $h_{pq}^{(Q)}(t)$ are defined as in (49) and (50), respectively. The angles of departures and the angles of arrivals are chosen as follows:

$$\alpha_T^{(m)} = 0.5\left(\frac{2\pi m}{M} + \frac{\psi - \pi}{M}\right) \tag{55}$$

$$\alpha_R^{(n)} = \frac{2\pi n}{N} + \frac{\theta - \pi}{N} \tag{56}$$

for $m = 1, \ldots, M$, $n = 1, \ldots, N$, respectively. The parameters ϕ_{mn}, β_m, β_n, θ, and ψ are independent random variables uniformly distributed on the interval $[-\pi, \pi)$. Our statistical model can be shown to exhibit properties (36) and (37) of the reference model. Derivations are omitted for brevity.

V. Simulation Results

This section presents simulation results of our new models. In all simulations, we use a normalized sampling period $f_{T\max}T_s = 0.01$ ($f_{T\max} = f_{R\max}$ are the maximum Doppler frequencies and T_s is the sampling period). The orientations of the $\mathrm{T_x}$ and $\mathrm{R_x}$ antenna arrays are chosen to be $\theta_T = \theta_R = \pi/2$. The angles of motion for the $\mathrm{T_x}$ and $\mathrm{R_x}$ are chosen to be $\gamma_T = \pi/4$ and $\gamma_R = 0$, respectively. The Rice factor is $K = 0.2$ and the AoA of the specular component is $\alpha_{Rq}^{LoS} = \pi$.

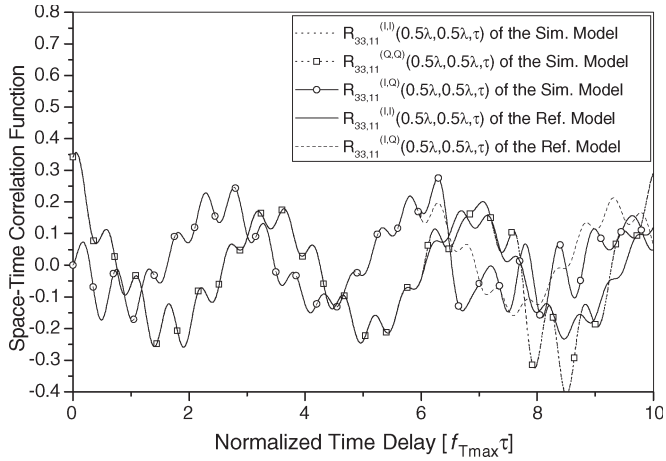

Fig. 6. Theoretical and simulated normalized space-time correlation functions of the I and Q components of the deterministic model for the radio propagation in outdoor micro-cells.

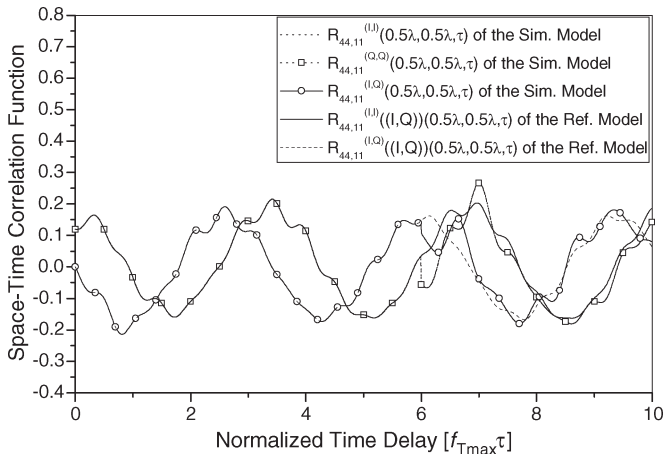

Fig. 7. Theoretical and simulated normalized space-time correlation functions of the I and Q components of the deterministic model for the radio propagation in outdoor macro-cells.

Figs. 6 and 7 present the space-time correlation functions ($\delta_T = \delta_R = 0.5\lambda$) of the I and Q components of the complex faded envelope, respectively, for system with $L_t = L_r = 4$ antennas, using $M = 22$ and $N = 40$ scatterers in the deterministic model. In Fig. 6, we assume that the single-bounced rays bear more energy than the double-bounced rays, i.e., $\eta_T = 0.7$, $\eta_R = 0.2$, and $\eta_{TR} = 0.1$. In Fig. 7, we assume that the double-bounced rays bear more energy than the single-bounced rays, i.e., $\eta_T = \eta_R = 0.2$ and $\eta_{TR} = 0.6$. Results show that the space-time correlation functions of the deterministic model approach the theoretical ones in the range of normalized time delays, $0 \leq f_{T\max}T_s \leq 6$.

Figs. 8 and 9 present the space-time correlation functions ($\delta_T = \delta_R = 0.5\lambda$) of the I and Q components of the complex faded envelope, respectively, for a system with $L_t = L_r = 4$ antennas, using $N = M = 16$ scatterers and $N_{\mathrm{stat}} = 50$ simulation trials in the statistical model. In Fig. 8, we assume that $\eta_T = 0.5$, $\eta_R = 0.4$, and $\eta_{TR} = 0.1$, whereas in Fig. 9, we assume that $\eta_T = \eta_R = 0.05$ and $\eta_{TR} = 0.9$. Results show that the space-time correlation functions of the statistical model approach the theoretical ones in the range of normalized time delays, i.e. $0 \leq f_{T\max}T_s \leq 10$.

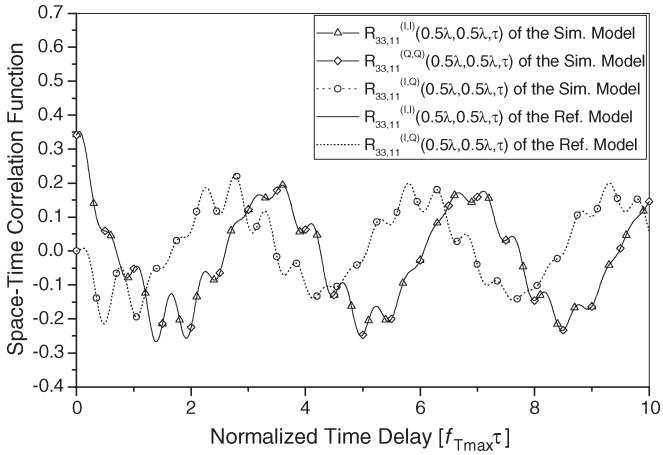

Fig. 8. Theoretical and simulated normalized space-time correlation functions of the I and Q components of the statistical model for the radio propagation in outdoor micro-cells.

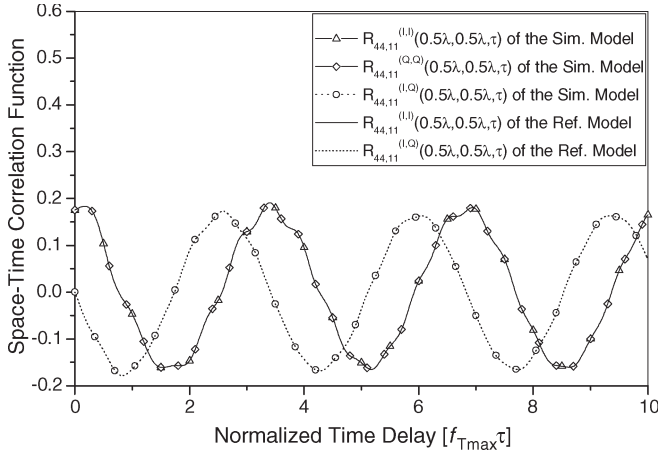

Fig. 9. Theoretical and simulated normalized space-time correlation functions of the I and Q components of the statistical model for the radio propagation in outdoor macro-cells.

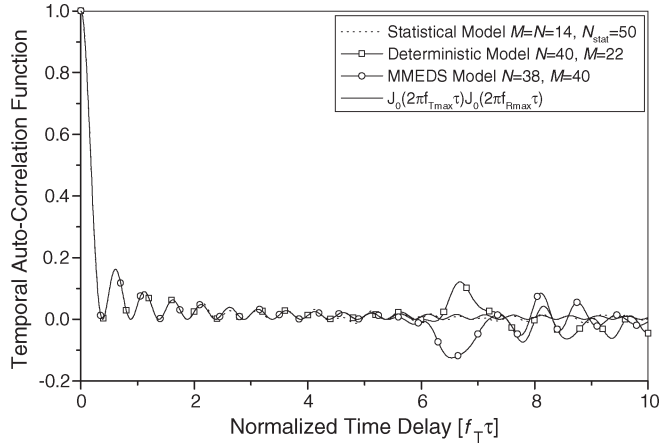

Fig. 10. Normalized temporal auto-correlation function ($\delta_T = \delta_R = 0$) of the complex faded envelope of the statistical, deterministic, MMEDS, and reference model.

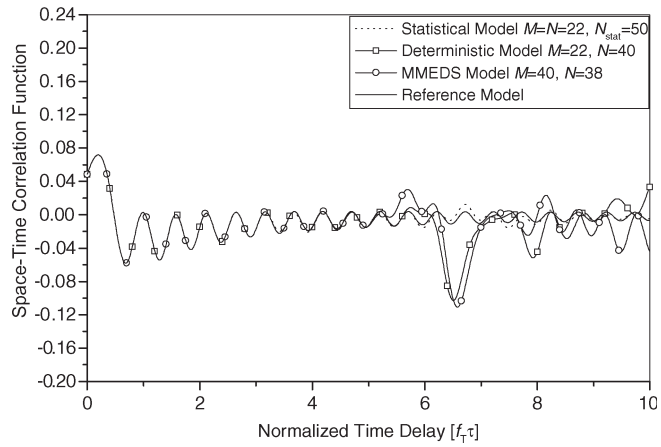

Fig. 11. Normalized space-time correlation function ($\delta_T = \delta_R = 1\lambda$) of the complex faded envelope of the statistical, deterministic, MMEDS, and reference model.

Here we compare the performance and complexity of our new models with the MMEDS model. For fair comparison, we remove the LoS and single-bounced components of the complex faded envelope from our models. Fig. 10 compares the temporal auto-correlation functions of the complex faded envelopes obtained by the deterministic, the statistical, and the MMEDS model. For the MMEDS model and the deterministic model, the temporal correlation functions are obtained using $M = 40,\ N = 38$ and $M = 22,\ N = 40$ scatterers, respectively. For the statistical model, the temporal correlation function is obtained using $N = M = 14$ scatterers and $N_{\text{stat}} = 50$ trials. Fig. 10 shows that the temporal correlation function of the MMEDS model approaches the theoretical one for normalized time delays in the range $0 \leq f_{T\max} T_s \leq 6$. The temporal correlation function of the deterministic model approaches the theoretical one in the same range of the normalized time delays as the MMEDS model, but requires a smaller number of scatterers. Finally, the temporal correlation function of the statistical model approaches the theoretical one in a wider range of normalized time delays (i.e., $0 \leq f_{T\max} T_s \leq 10$) than the deterministic and the MMEDS model.

Fig. 11 compares the space-time correlation functions of the complex faded envelopes for a system with $L_t = L_r = 2$ antennas, obtained by the deterministic, the statistical, and the MMEDS model. For the MMEDS model and the deterministic model, the space-time correlation functions are obtained using the same number of scatterers as in Fig. 10 and antenna distances $\delta_T = \delta_R = 1\ \lambda$. For the statistical model, the space-time correlation function is obtained using $N = M = 22$ scatterers, antenna distances $\delta_T = \delta_R = 1\ \lambda$, and $N_{\text{stat}} = 50$ trials. Fig. 11 shows that the space-time correlation function of the MMEDS model approaches the theoretical one for normalized time delays in the range $0 \leq f_{T\max} T_s \leq 5$. The space-time correlation function of the deterministic model approaches the theoretical one in a somewhat wider range of normalized time delays (i.e., $0 \leq f_{T\max} T_s \leq 6$), while requiring a smaller number of scatterers than the MMEDS model. The space-time correlation function of the statistical model approaches the theoretical one in the widest range of normalized time delays (i.e., $0 \leq f_{T\max} T_s \leq 10$).

Simulation results presented in Fig. 11 indicate that larger distances between antenna elements require a larger number of scatterers to match theoretical statistics for the same normalized time delays as in Fig. 10. For the statistical model, instead of using many scatterers (e.g., 40) in all simulations, we propose to adaptively select the number of scatterers depending on

TABLE I
COMPLEXITY OF DIFFERENT MODELS

Simulation models	Number of simulation trials	Estimated number of computations needed to generate $h_{pq}(t)$ (one simulation trial)				Relative simulation time needed to generate $h_{pq}(t)$
		number of scatterers	cosine	addition	random variable	
MMEDS Model	1	MN	$7MN$	$10MN$	MN	T
New Deterministic Model	1	$M_dN_d = MN/2$	$12M_dN_d = 6MN$	$14M_dN_d = 7MN$	$M_dN_d = MN/2$	$0.24T$
New Statistical Model	50	$M_sN_s \approx MN/25$	$12M_sN_s = 0.48MN$	$14M_sN_s = 0.56MN$	$M_sN_s + 2 = MN/25 + 2$	$0.95T$ (including averaging over 50 trials)

the distances between antenna elements. If we assume that a mean square error (MSE) of $\leq 10^{-3}$ is required for the simulated space-time correlation function of the complex faded envelope (relative to the theoretical one), we need at least $M = 14 + 2\lceil \delta_T/0.3\lambda \rceil$ and $N = 14 + 2\lceil \delta_R/0.3\lambda \rceil$ scatterers.[1] This methodology can also be applied to the deterministic and MMEDS models. However, to obtain similar statistics as with the statistical model, the number of scatterers needs to be larger, i.e., $70 + 10\lceil \delta_{T/R}/0.3\lambda \rceil$.

To compare complexity of the various models, Table I summarizes the number of simulation trials and the number of scatterers required to obtain similar statistical properties, the number of operations in one simulation trial needed to generate the complex faded envelope and the relative simulation times (including averaging over N_{stat} simulation trials) needed to generate the complex faded envelopes, in Matlab on a Pentium III laptop. Here, we count only the frequently executed operations and the number of random variables. Table I shows that the deterministic model has a lower complexity then the MMEDS model, whereas the statistical model has the highest complexity. Both of our new models require a smaller number of scatterers than the MMEDS model, which leads to shorter simulation times.

From Table I and Figs. 9–11 we can conclude that, our deterministic model performs similar to the MMEDS model, but has lower complexity and shorter simulation time. On the other hand, our statistical model, with slight increase in complexity, outperforms the deterministic and the MMEDS models. Finally, our deterministic and statistical model are more general and can be used to model various outdoor micro- and macro-cell propagation environments.

VI. CONCLUSION

This paper proposed the parametric reference model for MIMO mobile-to-mobile fading channels. From this model, the closed-form joint space-time correlation function and the space-Doppler power spectrum for a 2-D non-isotropic scattering environment are derived. Furthermore, the space-time correlation functions of the in-phase and quadrature components of the complex faded envelope for a 2-D isotropic scattering environment are derived. Finally, deterministic and statistical SoS simulation models for MIMO M-to-M fading channels are proposed. The statistical properties of the simulation models are verified by simulations. The results show that the simulation models are a good approximation of the reference model and that they outperform existing simulation models.

[1]Operation $\lceil \cdot \rceil$ denotes rounding up to the next integer.

APPENDIX
DERIVATIONS OF EQUATIONS (6)–(11)

From Fig. 1, using the cosine law, the distances ϵ_{pm}, ϵ_{mq}, ϵ_{pn}, and ϵ_{nq} can be written as

$$\epsilon_{pm}^2 = [(0.5L_t + 0.5 - p)\delta_T]^2 + R_T^2 - 2(0.5L_t + 0.5 - p)\delta_T R_t \cos\left(\theta_T - \alpha_T^{(m)}\right) \quad (57)$$

$$\epsilon_{mq}^2 = [(0.5L_r + 0.5 - q)\delta_R]^2 + \epsilon_m^2 - 2(0.5L_r + 0.5 - q)\delta_R \epsilon_m \cos\left(\alpha_R^{(m)} - \theta_R\right) \quad (58)$$

$$\epsilon_{pn}^2 = [(0.5L_t + 0.5 - p)\delta_T]^2 + \epsilon_n^2 - 2(0.5L_t + 0.5 - p)\delta_T \epsilon_n \cos\left(\theta_T - \alpha_T^{(n)}\right) \quad (59)$$

$$\epsilon_{nq}^2 = [(0.5L_r + 0.5 - q)\delta_R]^2 + R_R^2 - 2(0.5L_r + 0.5 - q)\delta_R R_r \cos\left(\alpha_R^{(n)} - \theta_R\right). \quad (60)$$

By applying the sine law to the triangles $\Delta O_T S_T^{(m)} O_R$ and $\Delta O_T S_R^{(n)} O_R$, respectively, we obtain following identities:

$$\frac{\epsilon_m}{\sin\alpha_T^{(m)}} = \frac{R_t}{\sin\left(\pi - \alpha_R^{(m)}\right)} = \frac{D}{\sin\left(\pi - \alpha_T^{(m)} - \left(\pi - \alpha_R^{(m)}\right)\right)} \quad (61)$$

$$\frac{R_r}{\sin\alpha_T^{(n)}} = \frac{\epsilon_n}{\sin\left(\pi - \alpha_R^{(n)}\right)} = \frac{D}{\sin\left(\pi - \alpha_T^{(n)} - \left(\pi - \alpha_R^{(n)}\right)\right)}. \quad (62)$$

From Fig. 1, we observe that $\pi - \alpha_R^{(m)} \leq \arcsin(R_t/D)$ and $\alpha_T^{(n)} \leq \arcsin(R_r/D)$. Based on the assumption $\min\{R_t, R_r\} \ll D$, we can conclude that $\arcsin(R_t/D) \approx R_t/D = \Delta_T$ and $\arcsin(R_r/D) \approx R_r/D = \Delta_R$, and consequently $\pi - \alpha_R^{(m)}$ and $\alpha_T^{(n)}$ are small angles. From (61) and (62), using approximations $\sin x \approx x$, $\cos x \approx 1$, and $\sqrt{1+x} \approx 1 + x/2$, for small x, the distances ϵ_{pm}, ϵ_{mq}, ϵ_{pn}, and ϵ_{nq} become

$$\epsilon_{pm} \approx R_t - \frac{(L_t + 1 - 2p)\delta_t}{2}\cos\left(\theta_T - \alpha_T^{(m)}\right) \quad (63)$$

$$\epsilon_{mq} \approx D - \frac{(L_r + 1 - 2q)\delta_R}{2}\left[\Delta_T \sin\theta_R \sin\alpha_T^{(m)} - \cos\theta_R\right] \quad (64)$$

$$\epsilon_{pn} \approx D - \frac{(L_t + 1 - 2p)\delta_T}{2}\left[\Delta_R \sin\theta_T \sin\alpha_R^{(n)} + \cos\theta_T\right] \quad (65)$$

$$\epsilon_{nq} \approx R_r - \frac{(L_r + 1 - 2q)\delta_R}{2}\cos\left(\alpha_R^{(n)} - \theta_R\right). \quad (66)$$

From Fig. 1, by applying the sine law to the triangle $\Delta S_T^{(m)} S_R^{(n)} O_R$, we obtain the following identity:

$$\frac{R_r}{\sin\chi} = \frac{\epsilon_{mn}}{\sin\left(\alpha_R^{(m)} - \alpha_R^{(n)}\right)} = \frac{\epsilon_m}{\sin\left(\pi - \chi - \left(\alpha_R^{(m)} - \alpha_R^{(n)}\right)\right)}. \quad (67)$$

From (67), using approximation $\sin x \approx x$ for small x, the distance ϵ_{mn} can be written as

$$\epsilon_{mn} = \epsilon_m \frac{\sin\left(\alpha_R^{(m)} - \alpha_R^{(n)}\right)}{\sin\left(\chi + \left(\alpha_R^{(m)} - \alpha_R^{(n)}\right)\right)} \approx D. \quad (68)$$

From Fig. 2, using the cosine low, the distance ϵ_{pq} can be written as

$$\epsilon_{pq}^2 = [(0.5L_r + 0.5 - q)\delta_R]^2 + \epsilon^2 - 2(0.5L_r + 0.5 - q)\delta_R \epsilon \cos\left(\alpha_{Rq}^{LoS} - \theta_R\right) \quad (69)$$

where $\epsilon^2 = [(0.5L_t + 0.5 - p)\delta_T]^2 + D^2 - 2(0.5L_t + 0.5 - p)\delta_T D\cos\theta_T$. Using the approximation $\sqrt{1+x} \approx 1 + x/2$, the distance ϵ_{pq} becomes

$$\epsilon_{pq} \approx D - (0.5L_t + 0.5 - p)\,\delta_T \cos\theta_T - (0.5L_t + 0.5 - q)\,\delta_R \cos\left(\alpha_{Rq}^{LoS} - \theta_R\right). \quad (70)$$

ACKNOWLEDGMENT

The authors would like to thank the anonymous reviewers whose feedback helped improve the quality of this paper.

REFERENCES

[1] A. S. Akki and F. Haber, "A statistical model of mobile-to-mobile land communication channel," *IEEE Trans. Veh. Technol.*, vol. VT-35, no. 1, pp. 2–7, Feb. 1986.

[2] A. S. Akki, "Statistical properties of mobile-to-mobile land communication channels," *IEEE Trans. Veh. Technol.*, vol. 43, no. 4, pp. 826–831, Nov. 1994.

[3] R. Wang and D. Cox, "Channel modeling for ad hoc mobile wireless networks," in *Proc. IEEE VTC*, Birmingham, AL, May 2002, vol. 1, pp. 21–25.

[4] C. S. Patel, G. L. Stüber, and T. G. Pratt, "Simulation of Rayleigh-faded mobile-to-mobile communication channels," *IEEE Trans. Commun.*, vol. 53, no. 11, pp. 1876–1884, Nov. 2005.

[5] A. G. Zajić and G. L. Stüber, "A new simulation model for mobile-to-mobile Rayleigh fading channels," in *Proc. IEEE WCNC*, Las Vegas, NV, Apr. 2006, vol. 3, pp. 1266–1270.

[6] J. Maurer, T. Fügen, and W. Wiesbeck, "Narrow-band measurement and analysis of the inter-vehicle transmission channel at 5.2 GHz," in *Proc. IEEE VTC*, Birmingham, AL, May 2002, vol. 3, pp. 1274–1278.

[7] G. Acosta, K. Tokuda, and M. A. Ingram, "Measured joint Doppler-delay power profiles for vehicle-to-vehicle communications at 2.4 GHz," in *Proc. IEEE GLOBECOM*, Dallas, TX, Nov. 2004, vol. 6, pp. 3813–3817.

[8] G. J. Byers and F. Takawira, "Spatially and temporally correlated MIMO channels: Modeling and capacity analysis," *IEEE Trans. Veh. Technol.*, vol. 53, no. 3, pp. 634–643, May 2004.

[9] M. Pätzold, B. O. Hogstad, N. Youssef, and D. Kim, "A MIMO mobile-to-mobile channel model: Part I—The reference model," in *Proc. IEEE PIMRC*, Berlin, Germany, Sep. 2005, vol. 1, pp. 573–578.

[10] B. O. Hogstad, M. Pätzold, N. Youssef, and D. Kim, "A MIMO mobile-to-mobile channel model: Part II—The simulation model," in *Proc. IEEE PIMRC*, Berlin, Germany, Sep. 2005, vol. 1, pp. 562–567.

[11] D. Gesbert, H. Bölcskei, D. A. Gore, and A. J. Paulraj, "Outdoor MIMO wireless channels: Models and performance prediction," *IEEE Trans. Commun.*, vol. 50, no. 12, pp. 1926–1934, Dec. 2002.

[12] J. Salz and J. H. Winters, "Effect of fading correlation on adaptive arrays in digital mobile radio," *IEEE Trans. Veh. Technol.*, vol. 43, no. 4, pp. 1049–1057, Nov. 1994.

[13] A. Abdi, J. A. Barger, and M. Kaveh, "A parametric model for the distribution of the angle of arrival and the associated correlation function and power spectrum at the mobile station," *IEEE Trans. Veh. Technol.*, vol. 51, no. 3, pp. 425–434, May 2002.

[14] K. I. Pedersen, P. E. Mogensen, and B. H. Fleury, "Power azimuth spectrum in outdoor environments," *Electron. Lett.*, vol. 33, no. 18, pp. 1583–1584, Aug. 1997.

[15] K. I. Pedersen, P. E. Mogensen, and B. H. Fleury, "A stochastic model of the temporal and azimuthal dispersion seen at the base station in outdoor propagation environments," *IEEE Trans. Veh. Technol.*, vol. 49, no. 2, pp. 437–447, Mar. 2000.

[16] I. S. Gradshteyn and I. M. Ryzhik, *Table of Integrals, Series, and Products*, 5th ed. A. Jeffrey, Ed. San Diego, CA: Academic, 1994.

[17] R. H. Clarke, "A statistical theory of mobile-radio reception," *Bell Syst. Tech. J.*, vol. 47, no. 6, pp. 957–1000, Jul./Aug. 1968.

[18] D. Shiu, G. J. Foschini, M. J. Gans, and J. M. Khan, "Fading correlation and its effect on the capacity of multielement antenna systems," *IEEE Trans. Commun.*, vol. 48, no. 3, pp. 502–513, Mar. 2000.

[19] A. Abdi and M. Kaveh, "A space-time correlation model for multielement antenna systems in mobile fading channels," *IEEE J. Sel. Areas Commun.*, vol. 20, no. 3, pp. 550–560, Apr. 2002.

[20] H. Kang, G. L. Stüber, T. G. Pratt, and M. A. Ingram, "Studies on the capacity of MIMO systems in mobile-to-mobile environment," in *Proc. IEEE WCNC*, Atlanta, GA, Mar. 2004, vol. 1, pp. 363–368.

[21] A. G. Zajić and G. L. Stüber, "Efficient simulation of Rayleigh fading with enhanced de-correlation properties," *IEEE Trans. Wireless Commun.*, vol. 5, no. 7, pp. 1866–1875, Jul. 2006.

[22] G. L. Stüber, *Principles of Mobile Communication 2E*. Norwell, MA: Kluwer, 2001.

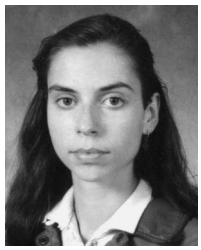

Alenka G. Zajić (S'99) received the B.Sc. and M.Sc. degrees from the School of Electrical Engineering, University of Belgrade, Belgrade, Serbia, in 2001 and 2003, respectively. From 2001 to 2003, she was a Design Engineer for Skyworks Solutions Inc., Fremont, CA. She is currently pursuing the Ph.D degree with the School of Electrical and Computer Engineering, Georgia Institute of Technology (Georgia Tech), Atlanta.

Since 2004, she has been a Graduate Research Assistant with the Wireless Systems Laboratory, Georgia Tech. Her research interests are in wireless communications and applied electromagnetics.

Ms. Zajić was recipient of the Dan Noble Fellowship in 2004, awarded by Motorola Inc. and the IEEE Vehicular Technology Society, for quality impact in the area of vehicular technology.

Gordon L. Stüber (S'81–M'82–SM'96–F'99) received the B.A.Sc. and Ph.D. degrees in electrical Engineering from the University of Waterloo, Waterloo, ON, Canada, in 1982 and 1986, respectively.

In 1986, he joined the School of Electrical and Computer Engineering, Georgia Institute of Technology, Atlanta, where he is the Joseph M. Pettit Chair Professor.

Dr. Stüber was co-recipient of the IEEE Vehicular Technology Society Jack Neubauer Memorial Award in 1997 for the best systems paper. He became an IEEE Fellow in 1999 for contributions to mobile radio and spread spectrum communications. He received the IEEE Vehicular Technology Society James R. Evans Avant Garde Award in 2003 for contributions to theoretical research in wireless communications. He served as General Chair and Program Chair for several conferences, including VTC'96, ICC'98, MMT'00, CTW'02, and WPMC'02. He is a past Editor for IEEE TRANSACTIONS ON COMMUNICATIONS (1993–1998) and served on the IEEE Communications Society Awards Committee (1999–2002). He was an elected member of the IEEE Vehicular Technology Society Board of Governors (2001–2003, 2004–2006) and received the Outstanding Service Award from the IEEE Vehicular Technology Society.